

Organic Ternary Solar Cells: A Review

Tayebeh Ameri,* Parisa Khoram, Jie Min, and Christoph J. Brabec

Recently, researchers have paid a great deal of attention to the research and development of organic solar cells, leading to a breakthrough of over 10% power conversion efficiency. Though impressive, further development is required to ensure a bright industrial future for organic photovoltaics. Relatively narrow spectral overlap of organic polymer absorption bands within the solar spectrum is one of the major limitations of organic solar cells. Among different strategies that are in progress to tackle this restriction, the novel concept of ternary organic solar cells is a promising candidate to extend the absorption spectra of large bandgap polymers to the near IR region and to enhance light harvesting in single bulk-heterojunction solar cells. In this contribution, we review the recent developments in organic ternary solar cell research based on various types of sensitizers. In addition, the aspects of miscibility, morphology complexity, charge transfer dynamics as well as carrier transport in ternary organic composites are addressed.

1. Introduction

The growing world energy demand has urged people to seek for new alternatives to conventional fossil resources. Photovoltaics offers the ability to generate electricity in a clean and renewable way. Among existing solar cells, organic photovoltaics (OPV) is one of the most promising technologies for the low cost energy production with the advantages of semi-transparency, flexibility and solution processing. Due to these beneficial and attractive features, a great deal of attention was given to research and development for higher OPV efficiency over the last few years. Recently, a significant breakthrough of over 10% power conversion efficiencies (PCEs) was reported on both polymer- and small molecule-based OPVs.^[1] Though impressive, further performance development is required to ensure a bright industrial future for OPVs.

Since organic semiconductors have a small dielectric constant, the primary excitation is mostly governed by resonating Frenkel excitons with a certain lifetime, typically in the order of

ns,^[2] and exciton binding energies much larger than the thermal energy. Thus, in view of photovoltaic charge generation, another driving force is needed to dissociate them. Blending conjugated polymers (donor) with high electron affinity molecules (acceptor) like fullerene derivatives, so-called bulk-heterojunction (BHJ) solar cells, is proven to be the most efficient way for rapid exciton dissociation (Figure 1a). As a result, the Voc of an organic solar cell (OSC) is governed by the highest occupied molecular orbitals (HOMO) of the donor material and the lowest unoccupied molecular orbital (LUMO) of the acceptor material obeying the following empirical equation:^[3]

$$V_{OC} = \frac{1}{e} \left(|E_{HOMO}^{Donor}| - |E_{LUMO}^{Acceptor}| \right) - 0.3 \quad (1)$$

Owing to this molecular excitonic nature of the primary excitation, absorption spectrum of organic conjugated polymers are restricted to a few 100 nm width instead of to a plateau absorption spectra, as seen for inorganic materials (Figure 1b). A detailed investigation of the donor absorption window and its influence on the OSCs performance was carried out by Minnaert et al.^[4] In an optimistic scenario with the assumption of 90% quantum efficiency (QE), 70% fill factor (FF) and 60% voltage factor (f), where $f = eV_{OC}/(|E_{HOMO}^{Donor}| - |E_{LUMO}^{Acceptor}|)$, the maximum efficiency was calculated as a function of the difference between the LUMO's of the donor and acceptor materials ($\Delta LUMO$) for different absorption windows (depicted in Figure 1c and 1d). The ideal bandgap (E_g) of the absorber for each absorption window was given for a LUMO-difference of 0 up to 0.5 eV. This study showed that for an empirical threshold of $\Delta LUMO = 0.2$ eV, expanding the absorption window from realistic width of 200 nm to an optimistic width of 400 nm resulted in a relative efficiency improvement of up to 35%.

To overcome the absorption limitation of the organic semiconductors, various strategies at different levels of maturity are currently in the exploration phase. For instance, design and synthesis of novel and high potential low-bandgap conjugated copolymers would extend light absorption and improve light harvesting.^[5] Alternatively, polymers with different bandgaps and absorption can be coupled into tandem cells.^[6] Tandem cells allow collecting photons resonant to the bandgap of either polymer, minimizing the thermalization losses. However, they are based on a complicated multi-layer stack with serious technical challenges. Among those challenges are the processing of a robust intermediate layer, the coupling of appropriate absorbers as well as the optimization of the active

Dr. T. Ameri, P. Khoram, J. Min, Prof. C. J. Brabec
Institute of Materials for Electronics
and Energy Technology (I-MEET)
Department of Materials Science and Engineering
Friedrich-Alexander University Erlangen-Nuremberg
Martensstrasse 7, 91058 Erlangen, Germany
E-mail: tayebeh.ameri@ww.uni-erlangen.de

Prof. C. J. Brabec
Bavarian Center for Applied Energy Research (ZAE Bayern)
Am Weichselgarten 7, 91058 Erlangen, Germany

DOI: 10.1002/adma.201300623



layers' thicknesses. Recently, an elegant alternative strategy was realized to extend the spectral sensitivity of wide bandgap polymers into the near IR region, the so-called organic ternary solar cell. In a ternary organic solar cell, an IR sensitizer is simply added to the host system consisting of a wide bandgap polymer blended with fullerene derivative, as it is illustrated in **Figure 2**. The ternary approach would not tackle the detailed balance limit,^[7] but rather improve the photon harvesting in thickness limited photoactive layers, resulting in higher short circuit current densities (J_{sc}) and therefore higher PCEs in a simple single-junction. As such, the ternary solar cell concept avoids the demanding challenges of multi-junction solar cells processing for spectrally broad light harvesting. However, it does so at a lower thermodynamic potential as a tandem cell.

OPV has to become a true-low-cost technology for the market competitiveness; not only for niche markets, but also for mainstream grid connected PV systems. So far, most of the high efficiency records are based on expensive materials which are frequently complex to scale up. Besides that, the majority of high efficient low bandgap polymers exhibit charge carrier recombination kinetics which are close to Langevin type behavior. These polymers can therefore only be coated in thin films which in turn limits light harvesting. On the other hand, according to literature evaluation, poly(3-hexylthiophene) (P3HT) blended with different types of fullerene derivatives, is the most-studied and most-used active material around the world for the bulk-heterojunction solar cells. Dang et al.^[8] have declared a number of around 1033 publications dealing with OPVs based on P3HT:1-(3-methoxycarbonyl)propyl-1-phenyl[6,6]C₆₁ (PCBM) between 2002 and 2010 (**Figure 3**). P3HT is well known for its high crystallinity and relatively good charge-transport properties among the different conjugated polymers. Even more important, it is one of the most accessible materials with defined quality and at reasonable price. As a big advantage, P3HT is exclusively functional with many different multi-adduct fullerene derivatives leading to the higher V_{oc} . All these advantages of P3HT strengthen the idea of further improving P3HT-based solar cells by co-sensitizing as an alternative approach to the development of novel high potential (co)polymers. Indeed, the near IR sensitizer can be based on the various types of materials such as low bandgap polymers, small molecules, dyes or nanoparticles (NP).

In this article we present a review on organic ternary solar cells reported by different research groups. The first part discusses the core concept of ternary solar cell operation, namely the different possible mechanisms of charge transfer and charge transport among the three components. Then, we present and discuss the reported experimental results on ternary solar cells, including all types of sensitizers. In addition, further aspects of the ternary solar cell concept, like miscibility, morphology complexity and processing are briefly addressed in the last section.

2. Charge Transfer and Transport Mechanisms

In general, a ternary solar cell consists of a wide bandgap polymer as the host donor, a near IR sensitizer and a fullerene derivative as the host acceptor. The charge transfer



Tayebeh Ameri received her MSc in Solid State Physics from Ferdowsi University of Mashhad, Iran. In 2010 she completed her PhD study in Engineering Sciences at Konarka Austria under the supervision of Prof. Christoph. J. Brabec (Konarka) and Prof. Kurt Hingerl (Johannes Kepler University Linz, Austria). Since October 2010, she is a postdoctoral fellow in the group of Prof. Brabec in the Institute of Materials for Electronics and Energy Technology (i-MEET) at the Friedrich Alexander University Erlangen-Nürnberg, where she leads the organic photovoltaics team. Her main research interests include investigation and development of ternary and tandem organic solar cells.



Parisa Khoram carried out her undergraduate studies at Ferdowsi university of Mashhad in Materials Science and Engineering. Since September 2011, she is a M.Sc. (Hons.) candidate of the Elite graduate program of Advanced Materials and Processes (MAP) at the Friedrich Alexander University Erlangen-Nürnberg. Currently, she is doing her master thesis on the topic of organic ternary solar cells under supervision of Prof. Brabec and Dr. Ameri.



Jie Min got both his B.S. degree (2008) and M. S. degree (2011) from China University of Mining and Technology, Beijing. During his master study he focused on the design and synthesis of polymers in organic electronics at the Institute of Chemistry, Chinese Academy of Sciences and Professor Yongfang Li as a Joint Master. Now he is a PhD student at the Friedrich-Alexander-university of Erlangen-Nuremberg under the supervision of Prof. Brabec. His research interests are in organic small molecules for electronics and photonics.



Christoph J. Brabec is holding the chair "Materials for Electronics and Energy Technology (i-MEET)" at the materials science department of the Friedrich Alexander University Erlangen-Nürnberg. Further, he is the scientific director of the Erlangen division of the Bavarian research institute for renewable energy (ZAE Bayern, Erlangen), board member of the ZAE Bavaria, and board member of the Energy Campus Nürnberg. He received his PhD (1995)

in physical chemistry from Linz university, joined the group of Prof Alan Heeger at UCSB for a sabbatical, and continued to work on all aspects of organic semiconductor spectroscopy as assistant professor at Linz university with Prof. Serdar Sariciftci. He joined the Siemens research labs as project leader for organic semiconductor devices in 2001, finished his habilitation in physical chemistry in 2003 at Linz university and joined Konarka in 2004, where he was holding the position of CTO before joining university. His research interests are organic photovoltaics, all aspects of solution processed semiconductors and technologies for renewable energy scenarios.

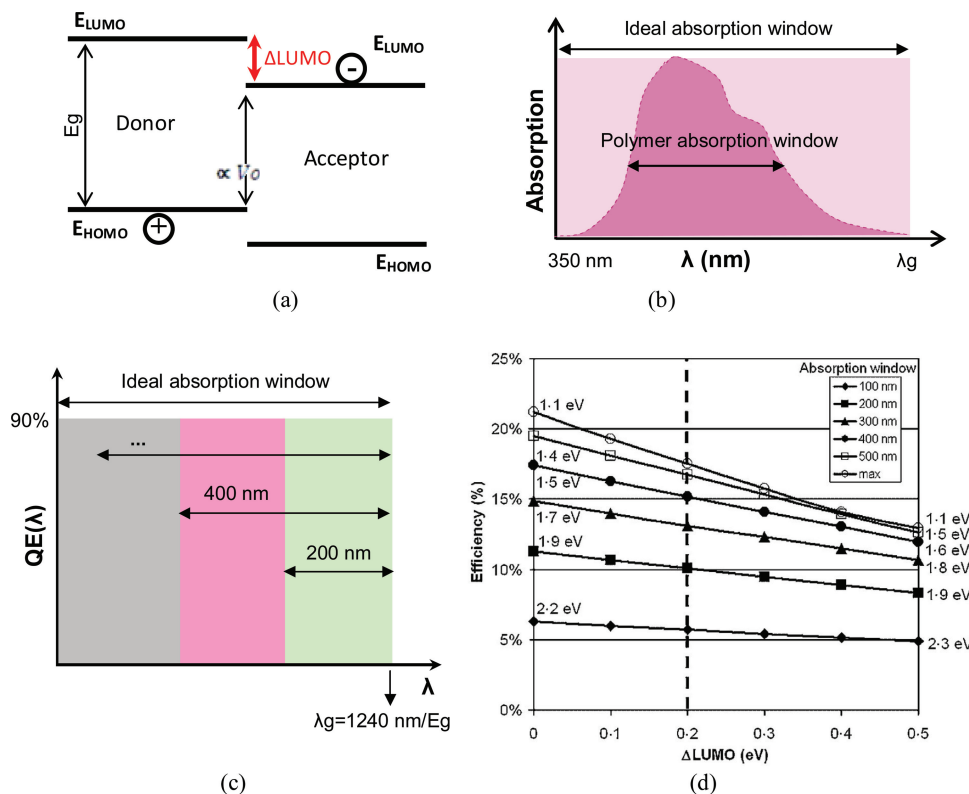


Figure 1. (a) Schematic energy band diagram of a bulk heterojunction single junction organic solar cell; (b) Illustration of the full/ideal absorption window compared to the narrow absorption window of polymers; (c) Definition of the optimistic scenario in the Minnaert et al.^[4] calculations: $\text{QE} = 90\%$, $\text{FF} = 70\%$ and $f = 60\%$ with different absorption windows. The cut-off wavelength λ_g corresponds with the bandgap E_g ; (d) The maximum efficiency in the optimistic scenario as a function of the difference between the LUMO's of the donor and acceptor materials for different absorption windows. The ideal bandgap of the absorber for each absorption window is given for a LUMO-difference of 0 up to 0.5 eV. The dotted line indicates the empirical threshold of 0.2 eV.^[4] Reproduced with the permission from Ref. [4].

and transport in the ternary blend is more than a simple superposition of the charge transfer and transport properties of the individual phases. It is governed by various mechanisms, depending on the sensitizer content, electronic energy levels and bandgap of the three components, sensitizer location in the binary photoactive layer as well as final microstructure of the film. Here, we present and discuss the main mechanisms reported so far.

2.1. Cascade Charge Transfer

The relative energetic position of the sensitizer's electronic levels with respect to those of host donor and acceptor determines the feasibility of a cascade exciton dissociation and charge transfer at the donor/sensitizer and sensitizer/acceptor interfaces. Locating the HOMO and LUMO level of the sensitizer between the HOMOs and LUMOs of host components

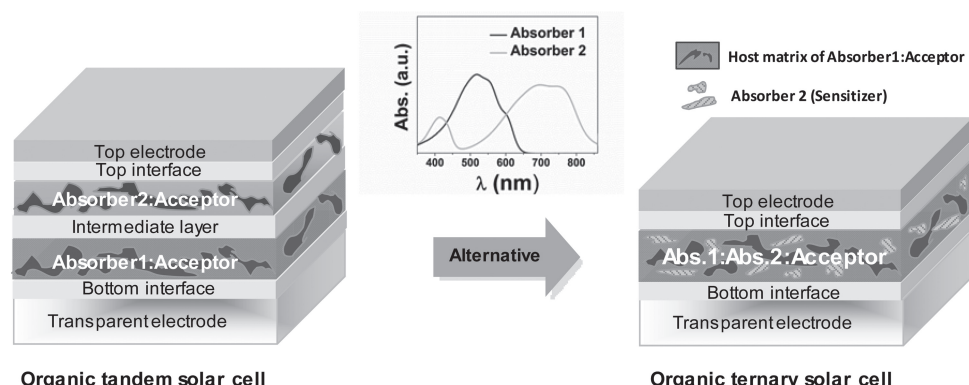


Figure 2. Schematic representation of an organic ternary solar cell, comprised of two absorbers with the complementary absorption spectra blended in fullerene derivatives, as an alternative for the tandem devices.

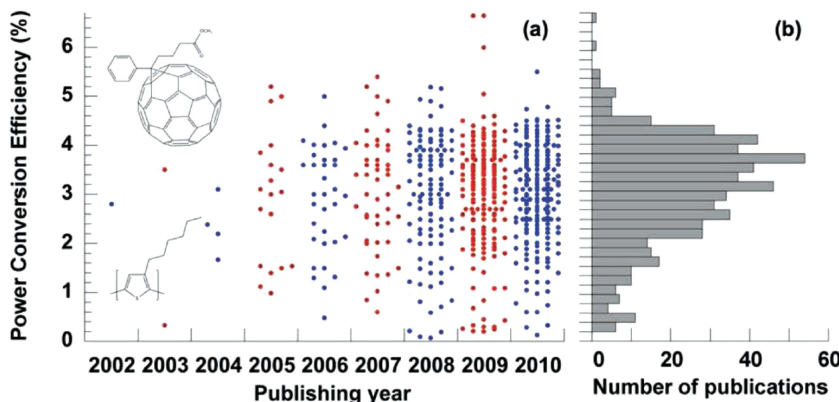


Figure 3. a) Power conversion efficiencies of the P3HT:PCBM-based solar cells reported in each of the 579 publications screened in the survey of Dang et al.^[8] Each dot corresponds to the maximum PCE value reported in each publication. The inset shows the chemical structures of P3HT and PCBM; b) The overall distribution of PCE values from 2002 to 2010.^[8] Reproduced with the permission from Ref. [8].

(cascade energy levels), several pathways are energetically relevant for the relaxation of photoexcited states. The photoexcited host donor may transfer an electron to either acceptor or the sensitizer phase instead. In the latter case, the sensitizer subsequently has to transfer an electron to acceptor. Alternatively, a photoexcited sensitizer can transfer a hole to host donor and in parallel an electron to the host acceptor. **Figure 4** illustrates this cascade charge transfer in a ternary blend.

This mechanism was reported by Koppe et al.,^[9] where P3HT:PCBM blend was employed as the host matrix and the low bandgap polymer of poly[2,6-(4,4-bis(2-ethylhexyl)-4H-cyclopenta[2,1-b;3,4-b']dithiophene)-alt-4,7-(2,1,3-benzothiadiazole)] (PCPDTBT or C-PCPDTBT) as the near IR sensitizer. Photoinduced absorption spectroscopy studies (PIA) revealed that photoexciting PCPDTBT (pump energy of 1.59 eV) in ternary P3HT:PCPDTBT:PCBM (0.8:0.2:1 wt.%) composites created free charges on P3HT. This near-IR (1.59 eV) photogeneration mechanism was absent in a binary blend made of P3HT:PCBM (1:1), shown in **Figure 5a**. Most importantly, these

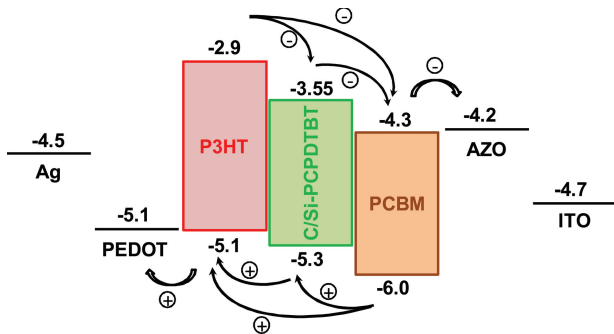


Figure 4. Schematic representation of the cascade charge transfer in a ternary solar cell, where the P3HT:PCBM is employed as the host system and low bandgap material of C-Si-PCPDTBT as the near IR sensitizer. The electronic energy levels of electrodes and semiconductors used in the study published in Ref. [25] are presented in eV unit. Curved arrows indicate allowed charge transfer reactions in the ternary blend. Reproduced with the permission from Ref. [25], Copyright 2012, Wiley.

PIA studies were the first indirect evidence that photogeneration of P3HT⁺ polarons can result from a hole transfer from a near-IR sensitizer (i.e. PCPDTBT) to P3HT. **Figures 6** and **6b** sketch two possible models of charge generation in P3HT:PCPDTBT:PCBM ternary films upon exciting PCPDTBT. In **Figure 6a**, diffusion of holes in PCPDTBT domains is involved in the charge generation process. Initially, excitons are created in PCPDTBT before electrons are transferred from PCPDTBT to PCBM, followed by a diffusion of holes in the PCPDTBT domains to an interface between PCPDTBT and P3HT, where finally holes are transferred from PCPDTBT to P3HT. In contrast to this model, no diffusion of holes is involved in the charge generation process lined out in **Figure 6b**.

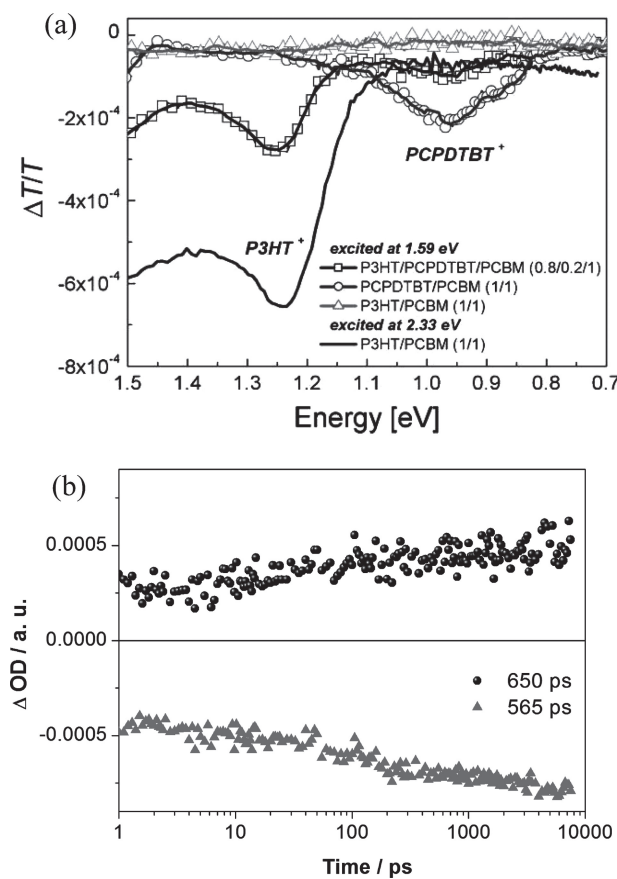


Figure 5. a) Photoinduced absorption spectra of annealed thin films ($d=100-150$ nm) of P3HT:PCPDTBT:PCBM (0.8:0.2:1) (open squares), PCPDTBT:PCBM (1:1) (open circles), and P3HT:PCBM (1:1) (open triangles) which were all excited at 1.59 eV. P3HT:PCBM (1:1), excited at 2.33 eV (full line), serves as a reference for the spectroscopic position of the P3HT polaron.^[9] Reproduced with the permission from Ref. [9]. b) Transient absorption profiles at 565 nm (triangle) and 650 nm (circle) of a P3HT:PCPDTBT:PCBM (0.9:0.1:1) film excited at 775 nm.^[10] Reproduced with the permission from Ref. [10].

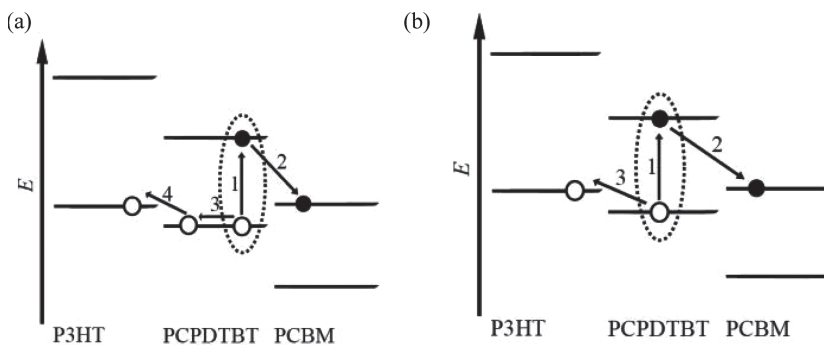


Figure 6. (a) Proposed mechanism of charge separation in ternary films with diffusion in PCPDTBT domains—including, firstly, generation of an exciton in PCPDTBT, secondly, electron transfer from PCPDTBT to PCBM, thirdly, hole diffusion to an interface between PCPDTBT and P3HT, and, fourthly, hole transfer from PCPDTBT positive polaron to P3HT; (b) Proposed mechanism of charge separation in ternary films without diffusion in PCPDTBT domains—including, firstly, generation of an exciton in PCPDTBT, secondly, electron transfer from PCPDTBT to PCBM, and, thirdly, hole transfer from PCPDTBT positive polaron to P3HT.^[10] Reproduced with the permission from Ref. [10].

Here, exciton generation in the PCPDTBT domains is followed by a coordinated exciton dissociation transferring an electron to PCBM while mutually transferring a hole to P3HT. Obviously, this mechanism is relevant for PCPDTBT units being assembled at the interface between PCBM and P3HT. In this regard, size and orientation of the sensitizer domains/chains is an decisive factor.

We have evaluated the hole transfer dynamics from PCPDTBT positive polarons to P3HT in P3HT:PCPDTBT:PCBM (0.9:0.1:1 wt.%) films upon excitation with a wavelength of 775 nm.^[10] Insights into hole transfer kinetics came from studying the photoinduced absorption transients at probe wavelengths of 650 and 565 nm as plotted in Figure 5b. The 650 and 565 nm features in the P3HT:PCPDTBT:PCBM films are ascribed to P3HT centered polarons and ground state bleaching of P3HT, respectively. Indeed, hole transfer starts at times faster than 1 ps, which is consistent with the mechanism of direct hole transfer. Hole transfer extends, nevertheless, throughout the investigated timescale of 7500 ps with a characteristic relaxation time of 140 ps. This slow decay times are consistent with the mechanism of hole transfer upon diffusion.

However, a well working ternary solar cell also requires a highly optimized charge transport matrix with very little charge recombination losses. The integrative mode Time of Flight (j-ToF) data, measured by Koppe et al.^[9], suggested that hole transport in the ternary blends dominantly occurs by the P3HT phase. It indicates that photocarriers generated on PCPDTBT are efficiently transferred to and subsequently transported via P3HT, while electrons are exclusively transported via the PCBM phase. In fact, this suggests that the optimum microstructure would position the sensitizer directly at the interface between the host donor and acceptor, as illustrated in Figure 7. On the one hand, it facilitates charge carrier transfer from the sensitizer into the host donor and acceptor matrices while preserving on the other hand the optimized transport properties of the host system.

Furthermore, we have shown that the effective sensitization of bulk heterojunction solar cells based on P3HT:PCBM blends by addition of Si analogue, poly[(4,40-bis(2-ethyl-

hexyl)dithieno[3,2-b:2',3'-d]silole)-2,6-diyl-alt-(4,7-bis(2-thienyl)-2,1,3-benzothiadiazole)-5,5'-diyl] (Si-PCPDTBT), follows very similar mechanism.^[11] The ternary blend of P3HT:Si-PCPDTBT:PCBM is also based on the rapid transfer of photogenerated positive polarons from the Si-PCPDTBT phase to the P3HT phase, leading to the depletion of the hole population on the low band gap polymer within few hundreds of picoseconds after the pump pulse. Intensity dependent experiments in combination with global fitting showed that the charge transfer from Si-PCPDTBT to P3HT competes with non-geminate charge carrier recombination of the holes in the Si-PCPDTBT phase with electrons in the PCBM phase, both processes being of diffusive nature. At excitation densities corresponding to steady state illumination from one sun, modeling predicts hole transfer efficiencies exceeding 90%.

2.2. Energy Transfer

Förster (Fluorescence) resonance energy transfer, resonance energy transfer or electronic energy transfer, is a mechanism describing energy transfer between two chromophores.^[12] A donor chromophore, initially in its electronic excited state, may transfer energy to an acceptor chromophore in its vicinity through non-radiative dipole–dipole coupling.^[13] For an energy transfer to occur, the acceptor molecule needs to have an absorption spectrum that overlaps with the emission spectrum of the donor molecule (Figure 8). This mechanism can become a relevant relaxation pathway for the primary photoexcited states in the ternary blends, depending on the domains sizes of the individual components. Photoluminescence measurement (PL) is a convenient tool to probe energy transfer.

PL studies suggested that energy transfer between P3HT to PCPDTBT is either absent or negligible in P3HT:PCPDTBT:PCBM blends. This most likely reflects the competition of the highly efficient photoinduced electron transfer reaction from P3HT to PCPDTBT.^[9] However, Honda et al.^[14] had reported considerable energy transfer from the host polymer P3HT to a silicon phthalocyanine derivative (SiPc) based near IR sensitizer in P3HT:SiPc:PCBM ternary composites by using transient absorption spectroscopy. Upon polymer excitation of the P3HT:SiPc:PCBM ternary blend (selective excitation of P3HT at 400 nm), a small and sharp depression was observed at around 680 nm as shown in Figure 9a, which otherwise was absent in P3HT:PCBM binary blends. This signal was ascribed to photobleaching of the SiPc ground state, which has a sharp absorption band at these energies. Figure 9b shows the time evolution of P3HT excitons (monitored at 1200 nm) and P3HT polarons (monitored at 650 to 1050 nm) in thermally annealed P3HT:PCBM binary and P3HT:SiPc:PCBM ternary composites. Interestingly, it was further observed that P3HT excitons decayed faster in the ternary blends than in the binary ones, suggesting that there is an alternative quenching

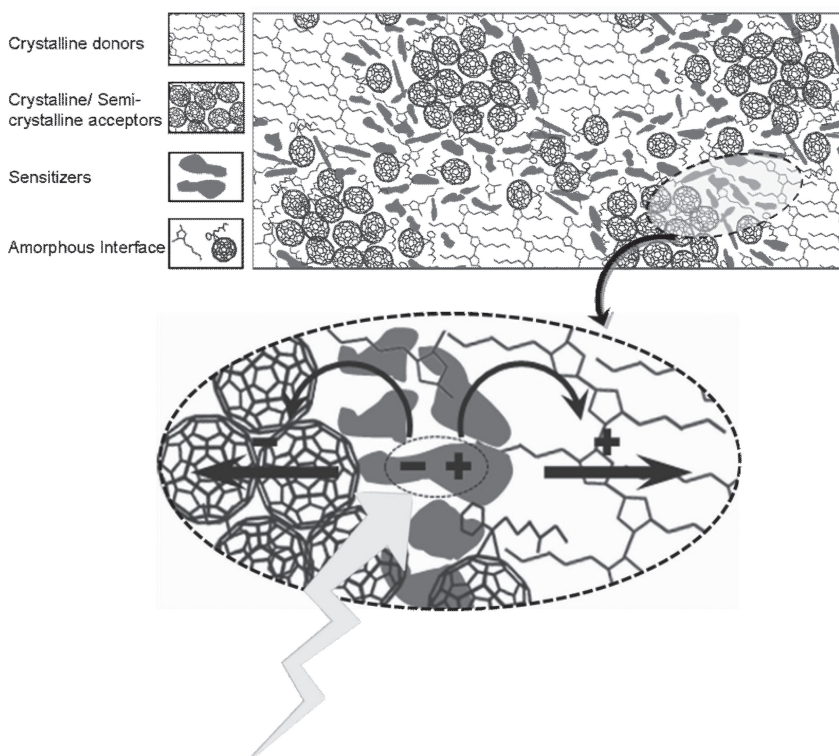


Figure 7. Illustration of an optimal microstructure of the ternary blends where the sensitizer positions directly at the interface between the host donor and acceptor. On the one hand, it facilitates charge carrier transfer from the sensitizer into the host donor and acceptor matrices while preserving on the other hand the optimized transport properties of the host system.

pathway for P3HT excitons in presence of SiPc. The transient analysis at 1200 nm revealed that app. half of the P3HT excitons are quenched with a lifetime of 4 ps in the presence of SiPc. The other half of the P3HT excitons decayed equally slow as in binary blends without SiPc. The generation rate of P3HT polarons (observed at 1000 nm) was determined to be 6 ps in the binary blends, which is actually slower than in the 4 ps measured for the ternary blends. This difference suggests the existence of a further intermediate state contributing to the generation of P3HT polarons. To address the origin of

this intermediate species, the photobleaching band of SiPc at 680 nm was investigated. As shown by the open circles in Figure 9b, the rise constant of the photobleaching band of SiPc was evaluated to be 4 ps. This is in good agreement with the decay constant of P3HT excitons and suggests that the rapid quenching of P3HT excitons in the ternary blends is due to an efficient energy transfer from P3HT excitons to SiPc. This energy transfer is favored due to the large spectral overlap between P3HT's emission and SiPc absorption. The fluorescence energy transfer from P3HT to SiPc was followed by a slightly delayed generation of P3HT polarons and SiPc anions from SiPc excitons (evaluated upon dye excitation). Subsequently, the photobleaching disappeared while the P3HT polaron band remained unchanged, suggesting subsequent charge transfer of the SiPc anion to PCBM (evaluated upon dye excitation). All these photovoltaic conversion processes were much more rapid than the backward reactions, and therefore highly efficient light harvesting was possible in this ternary blend composite. The authors further revealed that SiPc molecules are selectively positioned and localized at the interface between P3HT and PCBM, occupying up to 40% of the available interface sites.

Fluorescence energy transfer may also take place between the sensitizer to the host acceptor. Hesse et al.^[15] have reported fluorescence resonance energy transfer from a photoexcited dye to a fullerene. This effect was observed for an UV absorbing small molecule as well as for a near infrared absorbing polymer, namely hexa-peri-hexabenzocoronene (HBC) and PCPDTBT, in combination with a blend of 2,9-Di(pent-3-yl)-anthra[2,1,9-def:6,5,10-d'e'f']diisoquinoline-1,3,8,10-tetrone (PDI):PCBM. The steady state PL of PDI, PCBM and different mixtures of these molecules was measured upon excitation wavelength of 532 nm, where PDI absorbs strongly and PCBM weakly. The emission of PDI and PCBM is centered at 650 nm and 725 nm, respectively (Figure 10a). A clear trend was observed for all dye loading ratios: Emission at 725 nm (assigned to PCBM) was enhanced while perylene emission (at 600–650 nm) was strongly suppressed and shifted towards shorter wavelengths. This finding were explained by energy transfer from the perylene dye to PCBM. In both ternary systems, HBC/PDI:PCBM and PCPDTBT:PDI:PCBM, remarkably higher PCEs were achieved by this perylene sensitization of the fullerene. The unfavorable energy levels between PDI and PCBM suggest that cascade charge transfer reactions is absent or irrelevant (shown Figure 10b).

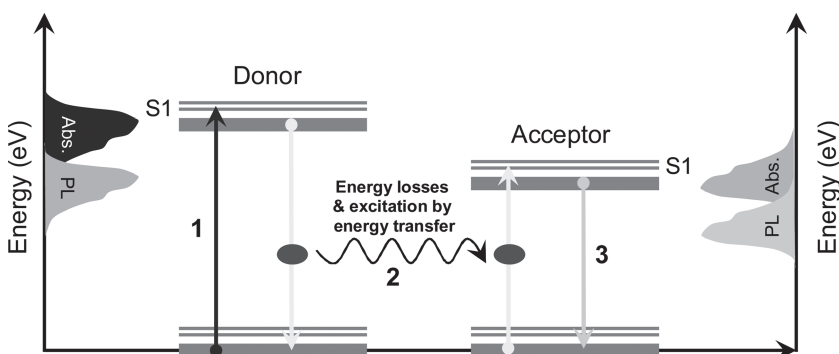


Figure 8. Schematic representation of the resonant energy transfer mechanism, as donor absorbs light (arrow 1) and transfers the energy to acceptor (arrow 2), which fluoresces (arrow 3). The abbreviations of Abs. and PL represent the absorption and photoluminescence spectra of the donor and acceptor, respectively.

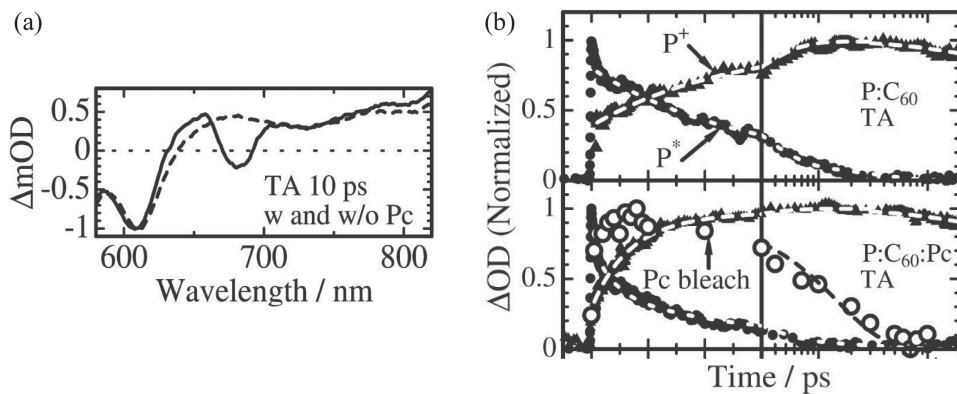


Figure 9. a) Magnified transient absorption spectra of thermal-annealed (TA) blend films at 10 ps with (—) and without (- - -) SiPc; b) Normalized transient absorption signals of P3HT:PCBM (top) and P3HT:SiPc:PCBM blend films (bottom) for thermal annealed films at 1200 nm (P3HT excitons; closed circles) and 1000 nm (P3HT polarons; closed triangles) excited at 400 nm. The open circles show the normalized rise fraction of the SiPc photobleaching. The broken lines are fitting curves to analyze the transient dynamics. In each panel, P, C60, and Pc represent P3HT, PCBM, and SiPc, respectively. Reproduced with the permission from Ref. [14]. Copyright 2011, American Chemical Society.

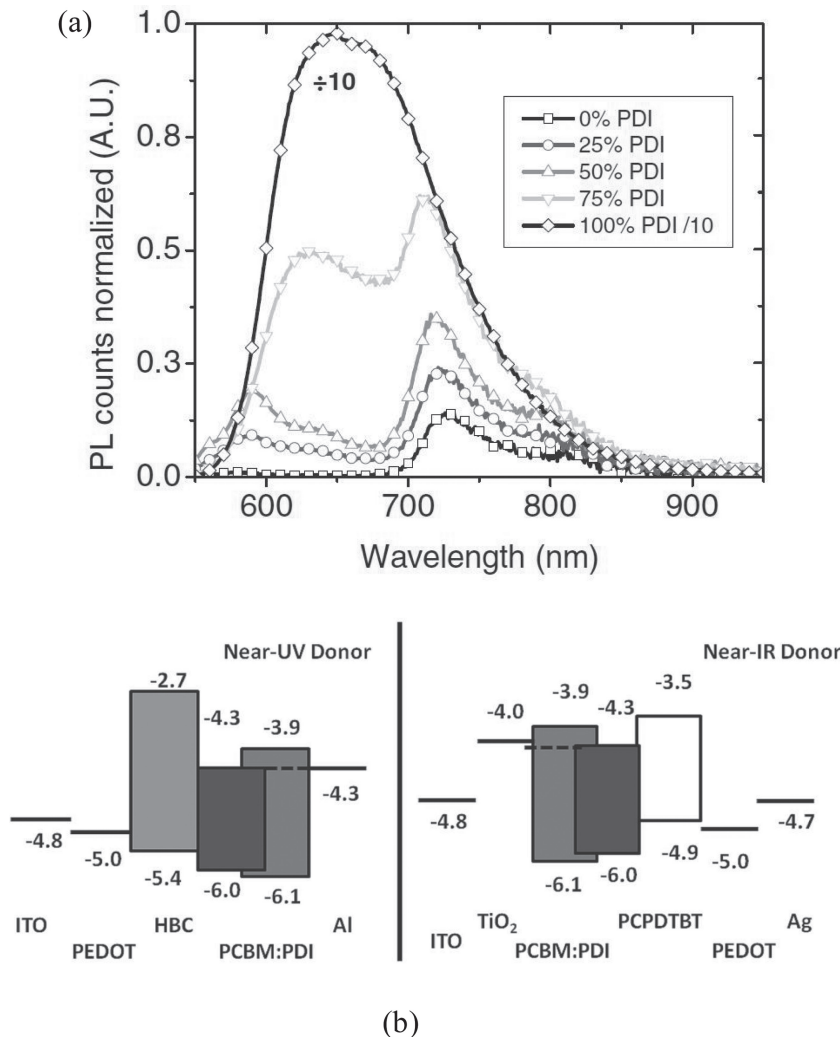


Figure 10. (a) Steady state photoluminescence spectra of PDI, PCBM and PDI:PCBM blend films, measured by Hesse et al.; (b) Schematic diagram of the energy levels for the materials used in study,^[15] where a fluorescence resonance energy transfer from PDI sensitizer to PCBM is reported. Reproduced with the permission from Ref. [15].

2.3. Parallel-Like Charge Transfer/Transport

Alternative to the cascade charge transfer mechanism, a parallel-like charge transport mechanism of two or more materials (mostly polymers) with different band gaps but similar polarity can be employed for the design of ternary systems. In this mechanism, excitons generated in each individual donor polymer would migrate to the respective polymer/acceptor interface and then dissociate into free electrons and holes. Electrons are transported via the acceptor domains towards the cathode as in normal binary solar cells. In the case that charge transfer between the two polymers is absent; holes will be transported towards the anode via the two parallel percolation pathways formed by the two polymers. (Figure 11). The charge carriers generated in each polymer:acceptor blend (or in each “sub-blend”) are collected simultaneously by the same cathode and anode electrodes, suggesting a photocurrent equal to the sum of those of the individual sub-blends. It is conceptually very similar to the parallel architecture of tandem devices and therefore such a single junction ternary system can be called parallel-like composite. The limiting factor of such a parallel-like system is the required transport capacity of both polymer absorbers.

Yang et al.^[16] reported the most efficient parallel-like BHJ ternary solar cells to date by employing poly(benzodithiophen-dithienylidifluorobenzothiadiazole) (DTffBT)^[17] and poly(benzodithiophene-dithienylthiadiazolo pyridine) (DTPyT),^[18] having different band gaps and HOMO levels as shown in Figure 12a. Solar cell composites were blended with PCBM at a weight ratio of

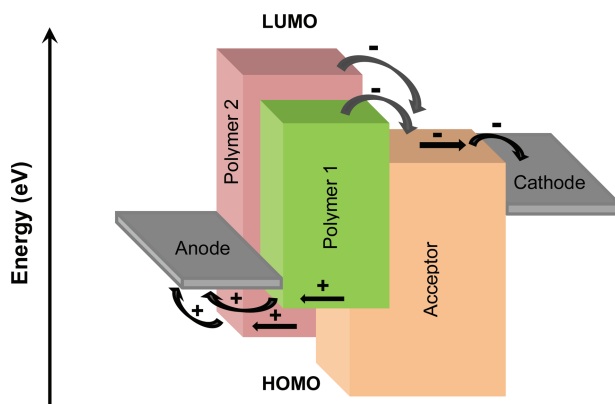


Figure 11. Schematic representation of the parallel-like charge transfer in a ternary solar cell, where polymer 1 and 2 are employed as the complementary absorbers blended in an acceptor. Curved arrows indicate charge transfer and linear arrows indicate charge transport in the ternary solar cell.

0.5:0.5:1. For better comparison, Yang et al. fixed the thickness of the ternary photoactive layer at 100 nm and for the binary reference cells at ~50 nm, neglecting possible interference effects from the back electrode. J_{sc} of the ternary devices was significantly increased (13.5 mA/cm^2) to almost the sum of the two binary reference cells (7.86 and 6.99 mA/cm^2 for DTffBT:PCBM and DTPyT:PCBM, respectively). V_{oc} of the ternary devices was between those measured for the individual binary devices. The J-V characteristics of the ternary and binary devices are shown in Figure 12b. Unlike other ternary systems that have a limitation of the sensitizer concentration, this parallel-like system exhibited enhanced performance at any blending ratio of the two polymers.

3. Review of Experimental Results

The concept of ternary organic solar cells is quite new and was reported first in 2009. However, the importance of this idea is

already acknowledged by many research groups and the development of ternary composites is in rapid progress. Various studies reported on fabrication methods, processing conditions, post treatments such as annealing and thickness of the photoactive layer, the choice for the third component, its properties and its concentration and their impact on the performance of ternary OSCs. For reviewing the experimental results, we distinguish between four types of sensitizers: low bandgap polymers, small molecules, dyes and nanoparticles.

This section reviews the main experimental findings for ternary solar cells with emphasis on the types of sensitizer. Further aspects of ternary composites like miscibility, morphology complexity and processing influence are also briefly addressed in this section.

3.1. Low Bandgap Polymer Sensitizers

The first demonstration of a ternary solar cells including a low bandgap polymer sensitizer was presented by Koppe et al.^[9] who sensitized P3HT:PCBM with 20 wt.% of the near IR absorber PCPDTBT. Annealing was required to optimize device performance. Without annealing, ternary devices suffered from low J_{sc} and FF compared to their binary reference. This indicated that the morphology of the pristine films was perturbed by the introduction of PCPDTBT to such an amount, that the formation of percolation pathways in P3HT:PCBM were impeded. However, at the highest PCPDTBT concentration of 20 wt.%, the gain in J_{sc} overcompensated the FF losses, which resulted in an absolute increase in efficiency.

By adding 20 wt.% PCDTBT into P3HT:PCBM, a constant external quantum efficiency (EQE) of around 15% was achieved for a wavelength range between 650 to 800 nm, where P3HT does not contribute to the photocurrent. Optimized ternary devices obtained PCEs of 2.8%, which was 10% higher than the performance of relevant binary reference. For PCPDTBT

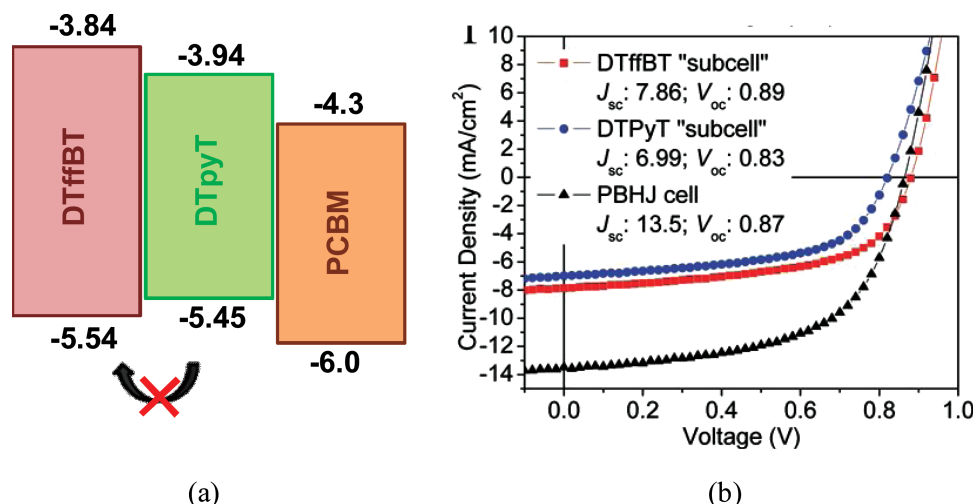


Figure 12. a) Schematic diagram of the energy levels for the materials used in Ref. [16], where parallel-like charges transfer mechanism is reported. The electronic energy levels are presented in eV unit; b) J-V characteristics of the parallel-like BHJ ternary cell (PBHJ) of DTffBT:DTPyT:PCBM and corresponding binary reference cells (subcells) of DTffBT:PCBM and DTPyT:PCBM. Reproduced with the permission from Ref. [16]. Copyright 2012, American Chemical Society.

contents significantly exceeding 20 wt.%, the drop in FF no longer was compensated by a J_{SC} gain, and the overall efficiency was not further increased.

An essential step towards understanding this prototype ternary blend was made by determining the solubility of all three components by assessing their Hansen solubility parameters (HSP).^[19] The design of multicomponent composites as well as formulations requires knowledge of the mutual solubility for all components. This information is easily extracted by analyzing separately the three solubility parameters δ_D (based on the atomic dispersive interactions), δ_P (based on the permanent dipole-permanent dipole molecular interactions) and δ_H (based on the molecular hydrogen bonding interactions). The cross-section of the individual solubility spheres of all three components determined the mutual solubility regime of P3HT, PCPDTB and PCBM (Figure 13). P3HT, which has a strong tendency to aggregate and the lowest solubility, was limiting the solubility for a composite ink for all three parameters of δ_D , δ_P , and δ_H . However, this limitation could be partially eased by applying higher temperatures. HSP analysis clearly suggested that there is sufficient compatibility between P3HT, PCPDTBT

and PCBM to be blended into one solution. As it is depicted in Figure 13, all these three components are soluble in a considerable number of common solvents at 60 °C with a solubility range of $\delta_D = 14.4\text{--}23.0$, $\delta_P = 0.0\text{--}5.7$ and $\delta_H = 0.5\text{--}8.8$ MPa^{1/2}.

Phase diagrams are common in polymer science to visualize the mixing behavior of multi-component systems as a function of temperature. Li et al.^[20] extracted the phase diagrams of P3HT, PCPDTBT and PCBM binary and ternary blends by employing differential scanning calorimetry (DSC). Figure 14a presents the phase diagram of binary and ternary blends for a large range of mixing ratios. The phase diagram of the binary system P3HT:PCBM showed a simple eutectic point at 60 wt.% P3HT content. Addition of small amounts of PCPDTBT did not significantly change the eutectic temperature of the ternary blends, which remained at a polymer:fullerene ratio of 60:40 wt.%. This is demonstrated by the existence of an eutectic channel (dark) along the composition of 40 wt.% PCBM in Figure 14a. Nevertheless, it was found that the crystallinity of ternary blends is slightly decreased at even low addition of the dominantly amorphous polymer PCPDTBT (0–20 wt.%). Higher PCPDTBT content generally led to even lower crystallinity.

Certain mixing ratios, e.g. at high PCBM or PCPDTBT concentrations, resulted in overall amorphous composites with no melting peaks (Figure 14b). Interestingly, the phase diagram reconstructed from DSC data, found good correlation between the thermal behavior of the semiconductor blends and their photovoltaic properties. Solar cells with a small content of PCPDTBT (<20 wt.%), located in the hypereutectic region, had high performance; the performance of solar cells including more than 20 wt.% PCPDTBT rapidly worsened and solar cells from amorphous ternary composites had outstanding poor electrical performance.

To analyze and understand the microstructure changes of P3HT:PCBM upon addition of PCPDTBT, further evaluation of the DSC traces turned out to be helpful.^[21] As it is shown in Figure 15a, the normalized enthalpy of P3HT:PCPDTBT, as determined by integrating the area beneath the P3HT melting peak, showed a linear relationship with nearly slope 1 as a function of PCPDTBT concentration. This shows that PCPDTBT obviously does not intercalate into the crystalline P3HT domains, but rather homogeneously mixes into the amorphous P3HT phase. The mixing behavior of PCBM and PCPDTBT was totally different. In contrast, the enthalpy of PCBM:PCPDTBT showed a significant drop in crystallinity upon addition of even small amounts of PCPDTBT. At above 30 wt.% PCPDTBT content no PCBM crystallinity is left. This proved that small amounts of PCPDTBT (0–20 wt.%) are mainly located in the amorphous matrix of P3HT:PCBM without affecting the

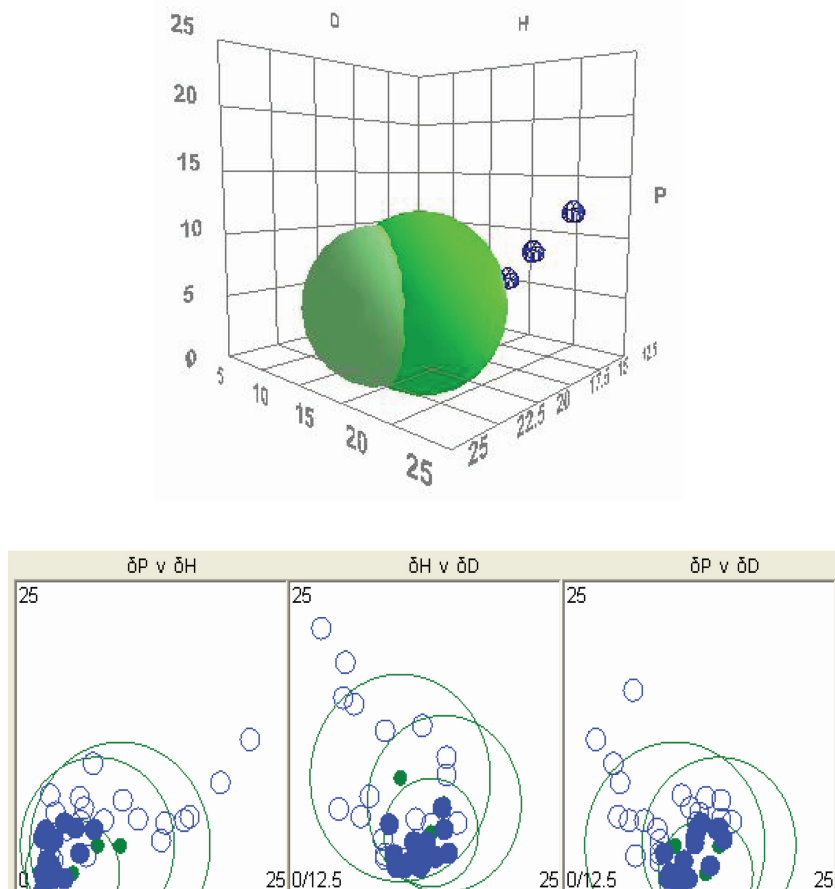


Figure 13. HSP diagram for solutes of P3HT, PCPDTBT and PCBM at 60 °C with 34 solvents and concentration of 2.5 g. L⁻¹ for the disperse parts (δ_D), polar parts (δ_P), and hydrogen-bonding parts (δ_H).^[19] All solvents within the cross-section of the three volumes (full symbols) are the common solvents for all three components. Reproduced with the permission from rRef. [19]. Copyright 2011, Wiley.

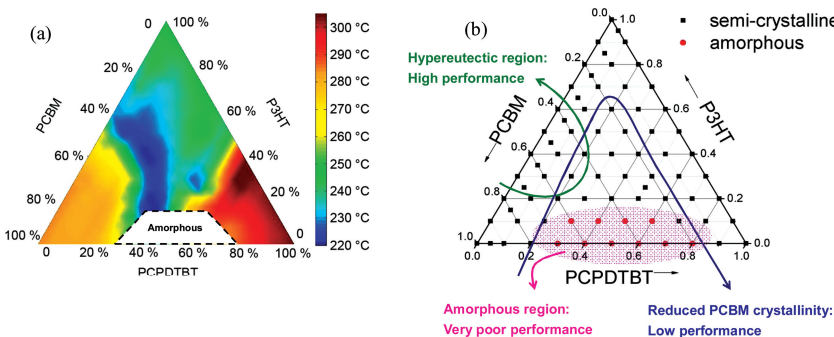


Figure 14. a) Phase diagram of binary and ternary blends of P3HT, PCPDTBT and PCBM, extracted from DSC first heating curves.^[20] b) Overview of phase behavior of binary and ternary blend mixtures, extracted from DSC first heating curves. Full squares stand for the crystalline mixtures, with melting peaks in DSC heating curves. Full circles represent amorphous mixtures. Three arrows present the correlations of the phase diagram to the high, low and very poor performance corresponding solar cells. Reproduced with the permission from Ref. [20]. Copyright 2011, Elsevier.

overall crystallinity of the system. Addition of more than 20 wt.% PCPDTBT results in a dramatic change and reduction in crystallinity, dominantly in PCBM crystallinity. Reduced PCBM crystallinity worsens electron transport, and consequently deteriorates solar cells performance. Figure 15b summarizes the microstructure evolution of P3HT:PCBM upon addition for PCPDTBT. This model was further supported by grazing incidence wide-angle x-ray scattering (GiWAXS) microstructure studies as well as space charge limited current (SCLC) transport measurements.^[21]

To reconstruct and tune the microstructure of P3HT:PCBM in the presence of PCPDTBT, Hu et al.^[22] applied 3 vol.% solvent additive of 1,8-diiodooctane (DIO) to the photoactive layer. This effect was reported to initiate stronger phase separation in binary PCPDTBT:PCBM blends and enhanced PCBM crystallinity.^[23] Contrary to that, Hu et al. attributed the morphology evolution of P3HT:PCPDTBT:PCBM in the presence of DIO to the reconstruction of P3HT crystallites rather than PCBM ones. Nevertheless, the addition of DIO resulted in P3HT:PCPDTBT:PCBM solar cells (1:0.2:1) with 20% increased J_{sc} and 17% increased device performance as compared to the optimized P3HT:PCBM reference. Overall, ternary solar cells with a maximum PCE of 3.33%, a J_{sc} of 12.67 mA/cm², a Voc of 0.55 V and a FF of 48% were reported.

Mikroyannidis et al.^[24] reported ternary solar cells based on copolymers of P (an alternating phenylenevinylene copolymer which contains 2-cyano-3-(4-(diphenylamino)phenyl)acrylic acid units along the backbone) and PB (a rather low bandgap alternating phenylenevinylene copolymer with BF2-azopyrrole complex units) blended in PCBM. The copolymers of P and PB show a maximum absorption at 420 and 511 nm with an optical bandgap of 1.94 and 1.63 eV, respectively. A ternary device of P:PB:PCBM with equal content of all components (1:1:1) yielded a PCE of 3.48% with J_{sc} = 7.5 mA/cm², Voc = 0.86 V and FF = 54% after thermal annealing. Indeed, thermal annealing enhanced the crystallinity of both P and PB and the hole mobility as well as the overall charge transport of the ternary blend was improved. Efficiency reported for the ternary devices exceeded the binary cells by over 50%. (PCEs

of P:PCBM = 1.6% and PCEs of PB:PCBM = 1.57%). Figure 16a summarizes the EQE spectra of the ternary cells. The identical LUMO level of P and PB (-3.45 eV) suggests that the parallel-like and/or energy transfer mechanisms may occur in this ternary system.

Recently, we had introduced the Si analogue of C-PCPDTBT, poly[(4,40-bis(2-ethylhexyl)dithieno[3,2-b':3',2-d]silole)-2,6-diyl-alt-4,7-bis(2-thienyl)-2,1,3-benzothiadiazole]-5,5'-diyl] (Si-PCPDTBT), into P3HT:PCBM blend as an alternative to the carbon bridged pendant PCPDTBT.^[25] Despite the chemical similarity of both compounds, ternary solar cell function differed significantly. J_{sc} showed a successive and linear enhancement with adding more Si-PCPDTBT even up to 70 wt%. Adding Si-PCPDTBT to a binary P3HT:PCBM composite affected the

Voc as well. A gradual increase of Voc versus the Si-PCPDTBT content was observed. From the energy level perspective, one would expect Voc to remain at the P3HT:PCBM value even for a ternary cell, since Voc is determined by the difference of the PCBM LUMO to the lowest-available polymer HOMO level. Contrary to this expectation, detailed investigations of the ternary P3HT:PCBM:ICBA^[26] composite showed that Voc is not limited to the smaller Voc of the binary solar cells but rather varied between the two binary Voc values. The Voc increase in the ternary solar cells was dominantly explained by the more favorable ratio of charge generation to charge recombination. The Voc of solar cells is expressed as:^[27]

$$V_{oc} \approx \frac{nkT}{q} \ln \left(\frac{J_{ph}}{J_0} \right) \quad (2)$$

where, n is the ideality factor, J_{ph} is the photocurrent density, and J₀ is the saturation current density. Therefore, a small and progressive improvement of Voc can be attributed to the enhanced photocurrent of the cells after sensitization. In addition, Schlenker et al.^[28] have demonstrated that the cascade donor structure is effective in decreasing J₀ through reducing nonradiative contributions to the recombination of the charge transfer (CT) state. It is a direct consequence of the reduction of electronic coupling at the donor/acceptor interfaces in cascade structures. Therefore, the slight Voc increase may as well originate from the reduction of J₀. Finally, a recent study of Thompson's group^[29] revealed that in ternary donor:donor:acceptor and donor:acceptor:acceptor composites, the donor:donor and acceptor:acceptor components form an alloy with HOMO and LUMO energies based on their average composition. Therefore, the CT state energy and consequently the Voc of the ternary solar cells vary as the composition of either the donors or acceptors is changed.

The variation of the FF in ternary devices of P3HT:Si-PCPDTBT:PCBM followed a puzzling trend whereas the FF is dominantly related to the microstructure influenced carrier recombination dynamics. Nevertheless, we found that the FF of ternaries' was comparable to (FF = 0.63) or even slightly higher (at 30 wt.% content of the sensitizer (FF = 0.66)) than the

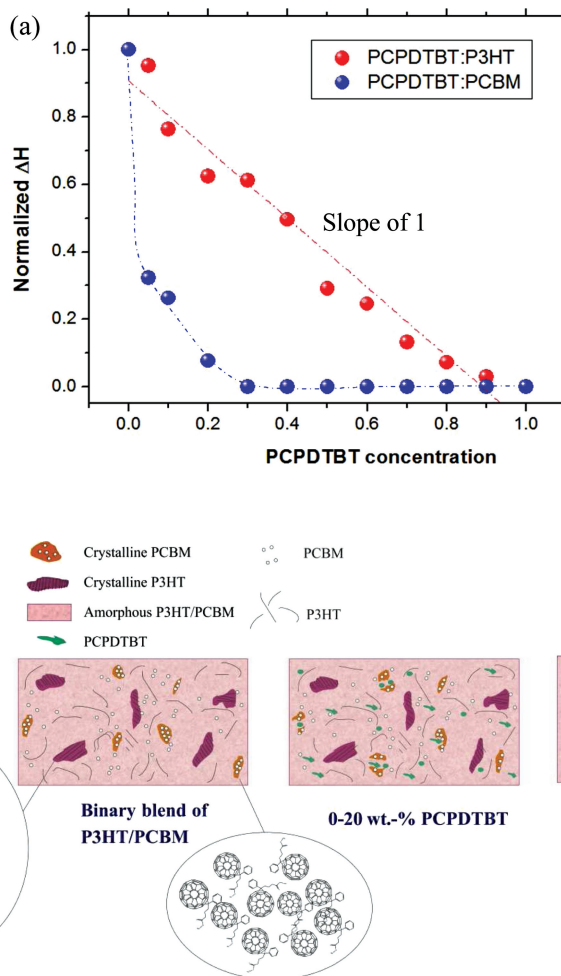


Figure 15. a) Normalized enthalpy change determined by integration of the P3HT and PCBM melting peak area in the binary blends of PCPDTBT:P3HT and PCPDTBT:PCBM, respectively; b) Schematic representation of the influence of PCPDTBT addition on morphology of the P3HT:PCBM binary blend.^[21] Reproduced with the permission from Ref. [21]. Copy right 2012, Royal Society of Chemistry.

binary P3HT:PCBM references at Si-PCPDTBT loadings of up to 40 wt.%. At Si-PCPDTBT contents higher than 50 wt.%, the FF dropped dramatically. Over all, inverted ternary cells with 30 wt.% Si-PCPDTBT reached PCEs exceeding 4% with $J_{sc} = 11 \text{ mA/cm}^2$, $Voc = 0.59 \text{ V}$ and $FF = 62\%$. This is an essential improvement compared to the 3% efficient binary P3HT:PCBM reference. The EQE spectra for P3HT:PCBM and for ternary cells with different content of the Si-PCPDTBT, presented in Figure 16b, proved the successful and efficient near IR sensitization with Si-PCPDTBT. Obviously, P3HT:PCBM sensitization with Si-PCPDTBT works very different than C-PCPDTBT sensitization. Such a high sensitizer concentration of 40 wt.% without significant FF losses demonstrates that Si-PCPDTBT does not damage the complex P3HT:PCBM microstructure. Parallel like transport are likely to occur at these high sensitizer concentrations of 40%.

In another study, Khlyabich et al.^[30] investigated ternary solar cells containing two P3HT analogue donors, a high band-gap poly(3-hexylthiophene-co-3-(2-ethylhexyl)thiophene) (P3HT₇₅-co-EHT₂₅) and low bandgap poly(3-hexylthiophene-thiophene-diketopyrrolopyrrole) (P3HTT-DPP-10%), blended in PCBM

as an acceptor. Optimizing the overall polymer:acceptor ratio for each polymer:polymer ratio, a linear increase of Voc with sensitizer content accompanied with high FF were observed. At the weight ratio of 0.9:0.1:1.1 for the P3HTT-DPP-10%:P3HT₇₅-co-EHT₂₅:PCBM composition, a PCEs of 5.51%, with a $J_{sc} = 15.05 \text{ mA/cm}^2$, $Voc = 0.6 \text{ V}$ and $FF = 61\%$ was achieved, exceeding those of the corresponding binary blends (5.07 and 3.16%). In this case, actually the low badgap polymer of P3HTT-DPP-10% acted as the host polymer, sensitized in the visible region by 10 wt.% P3HT₇₅-co-EHT₂₅ (Figure 16c).

Afterward, Yang et al.^[16] reported two individual ternary solar cells based on different groups of novel copolymers blended in PCBM. The light harvesting of DTffBT:PCBM were improved with DTPyT as near IR sensitizers for the regime between 650 nm and 800 nm. As a result, the J_{sc} values for the ternary devices at all compositions were improved relative to the binary devices. Upon addition of DTPyT into the host blend, the Voc changed gradually from 0.91 to 0.85 V, i.e., between those values measured for the individual binary cells. The FF of the ternary devices remained as high as for the host system. Optimizing the photoactive layer thickness, the highest PCE

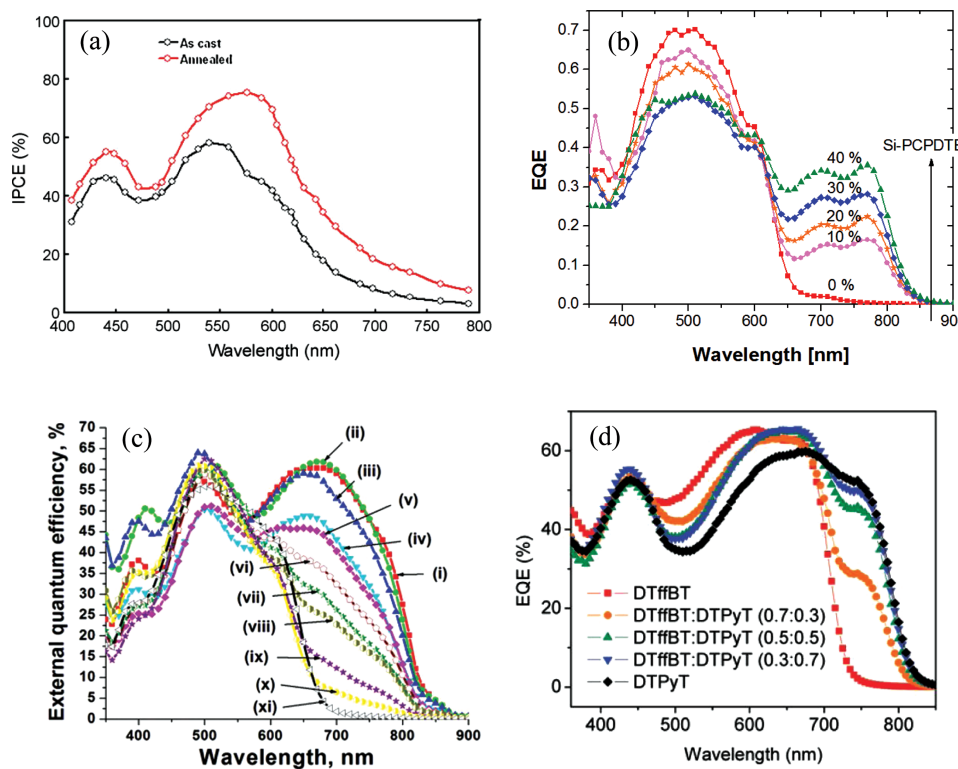


Figure 16. EQE spectra of the a) ternary solar cells based on P:PB:PCBM as cast and thermally annealed. Reproduced with the permission from Ref. [24]. Copyright 2011, Elsevier. b) binary cell of P3HT:PCBM (1:1) and ternary cells including 10, 20, 30 and 40 wt.% Si-PCPDTBT.^[25] Reproduced with the permission from Ref. [25]. c) ternary solar cells of P3HTT-DPP-10%:P3HT₇₅-co-EHT₂₅:PCBM with various ternary blend ratios: (i) 1:0:1.3, (ii) 0.9:0.1:1.1, (iii) 0.8:0.2:1.0, (iv) 0.7:0.3:1.0, (v) 0.6:0.4:1.0, (vi) 0.5:0.5:0.9, (vii) 0.4:0.6:0.9, (viii) 0.3:0.7:0.8, (ix) 0.2:0.8:0.8, (x) 0.1:0.9:0.9, and (xi) 0:1:0.8. Reproduced with the permission from Ref. [30]. Copyright 2012, American Chemical Society; d) binary cells of DTffBT:PCBM and DTPyT:PCBM and ternary cells including 30, 50 and 70 wt.% DTPyT in DTffBT:PCBM. Reproduced with the permission from Ref. [16]. Copyright 2012, American Chemical Society.

of 7.02% with a $J_{sc} = 13.7 \text{ mA/cm}^2$, $V_{oc} = 0.87 \text{ V}$ and $FF = 58.9\%$ was achieved for a DTffBT: DTPyT:PCBM ternary cell at a weight ratio of 0.5:0.5:1.

A second successfully optimized ternary system was composed of poly(benzodithiophene–dithienylbenzothiazole) (TAZ) and poly(benzodithiophene–dithienylbenzothiadiazole) (DTBT), blended in PCBM. TAZ and DTBT exhibit an absorption band of 450–650 and of 500–800 with the maximum peaks at around 580 and 700 nm, respectively. A similar composition-dependent device behavior was observed for this composition.. In particular, ternary devices consisting of a 0.3:0.7:1 weight ratio composite of TAZ:DTBT:PCBM showed a highest PCEs of 5.88% with $J_{sc} = 11.9 \text{ mA/cm}^2$, $V_{oc} = 0.81 \text{ V}$ and $FF = 60.68\%$. Also in this case it is the low bandgap polymer (DTBT,with 70 wt.% concentration) being dominant polymer with respect to composition and charge transport. A parallel-like charge transport was proposed for both prototype ternary systems, although the components' energy levels of the latter system did not exclude cascade charge transfer/transport or energy transfer mechanisms.

Further reports also reported UV sensitization rather than NIR sensitization. In 2009, Kim et al.^[31] had reported a ternary solar cell based on a P3HT:PCBM host matrix and poly(9,9-diptylfluorene-co-benzothiadiazole) (F8BT) as UV sensitizer.

The best ternary blend solar cell required annealing at 130 °C and exhibited a slightly higher performance (1.94%) than the F8BT:P3HT binary solar cell with equal P3HT composition (1.38%). However, ternary performance was lower than the optimized binary solar cell with the P3HT:PCBM (3.16%).

Adam et al.^[32] demonstrated that mixing of (poly{1,4-(2,5-diocyloxy)-phenyleneethynylene-2,5-thiophenylenevinylene-1,4-[[(5-(2-ethylhexyl)oxy)-2-methoxy]phenylenevinylene (DO-PThE1-PPV2) and poly{1,4-[[(2-ethylhexyl)oxy]-2-methoxy)-phenyleneethynylene-2,5-thiophenylenevinylene-1,4-[[(5-(2-ethylhexyl)oxy)-2-methoxy] phenylenevinylene} (MEH-PThE1-PPV2), consisting of the same conjugated backbone but different types and volume fraction of alkoxy side chains on the phenylene ethynylene unit, blended in PCBM resulted in a slight improvement over the binary references. This improvement was attributed to an enhanced charge carrier mobility in the DO-PThE1-PPV2:MEH-PThE1-PPV2 mixture ($\mu^{DO:MEH}_h = 2.6 \times 10^{-4} \text{ cm}^2/\text{Vs}$) as compared to the individual polymers ($\mu^{DO:PThE1}_h = 1.8 \times 10^{-5} \text{ cm}^2/\text{Vs}$, $\mu^{MEH - PThE1}_h = 2 \times 10^{-6} \text{ cm}^2/\text{Vs}$). A ternary solar cell of D1:D2:PCBM with a mixing weight ratio of 0.5:0.5:3 showed a PCE = 2% with $J_{sc} = 5.7 \text{ mA/cm}^2$, $V_{oc} = 0.86 \text{ V}$ and $FF = 40\%$.

Chen et al.^[33] introduced a small amount of the bipolar poly[2,3-bis(thiophen-2-yl)-acrylonitrile-9,9-diptyl-fluorene]

(FLC8) into a P3HT:PCBM host matrix, mainly with the target to improve the electrical transport properties of the matrix. The absorption peak of FLC8 is blue shifted by only 30 nm to P3HT. The PCEs of 2.93% with a $J_{sc} = 8.16 \text{ mA/cm}^2$, $V_{oc} = 0.68 \text{ V}$ and $FF = 52.8\%$ were achieved for the ternary device of P3HT:FLC8:PCBM for a weight ratio of 1:0.05:0.8. The 30% performance improvement of the ternary device compared to the P3HT:PCBM device is attributed to some additional charge separation to FLC8 but mainly due to improved charge transfer properties due to the ambipolarity of FLC8.

Recently, Lobe et al.^[34] designed a series of AB-alternating side-chain-functionalized poly(thiophene) analogues, P1-6, to selectively localize at the interface between regioregular P3HT and PCBM. The highest performance was achieved by implementing the analogue of P6 containing electron-deficient perfluorophenyl moieties. A 220 nm thick P3HT:PCBM device containing just 0.25 wt.% P6 gave PCEs of up to 5.3% with $J_{sc} = 21.3 \text{ mA/cm}^2$, $V_{oc} = 0.6 \text{ V}$ and $FF = 44\%$ (30% PCE increase over the reference device lacking P6). The authors had proposed that P6 selectively localized at the interface between P3HT and PCBM with the aromatic moieties in the side-chains introducing a dipole at the polymer/fullerene interface, which then decreased the rate of bimolecular recombination.

A brief summary of the reports dealing with ternary organic solar cells based on polymeric sensitizers is presented in Table 1. Figure 17 depicts the chemical structures of utilized materials in the photoactive layer of those ternary devices.

3.2. Small Molecule Sensitizers

Compared to polymeric semiconductors, molecular ones have several advantages such as well-defined structures, high intrinsic carrier mobility, no batch-to-batch variations, and ease of synthesis, purification, and modification. Therefore, they are a great candidate to be used in organic photovoltaics as the main component in a binary matrix as well as a sensitizer in a ternary composite.

In 2010, a ternary solar cell comprised of a novel developed conjugated small molecule sensitizer with the cascade structure was reported by Huang et al.^[35] The solution processed small molecule 7,70-[5,50-[10,12-bis(4-tert-butylphenyl)dibenzof[f,h]thieno[3,4-b]quinoxaline-2,7-diyl]bis(thiophene-5,2-diyl)]bis(9,9-dihexyl-N,N-diphenyl-9H-fluoren-2-amine) (TQTFA) was incorporated into a solar cell based on P3HT and (6,6)-phenyl-C71-butyric acid methyl (PC70BM). The absorption spectrum of compound TQTFA covered a broad spectral range from 300 to 650 nm. The absorption maximum appeared at a very short wavelength (420 nm), though the absorption coefficient at this wavelength ($1.8 \times 10^5 \text{ cm}^{-1}$) was as high as that of P3HT. The device comprising of 2:0.5:2 wt.% P3HT:TQTFA:PC70BM exhibited a highest PCE of 4.5% with a $J_{sc} = 10.62 \text{ mA/cm}^2$, $V_{oc} = 0.69 \text{ V}$ and $FF = 60.7\%$, which is around 13% improvement compared to the efficiency of the P3HT:PC70BM reference. The EQE spectrum of the P3HT:PC70BM based device was enhanced at wavelength range of 340–650 nm upon blending with TQTFA, particularly in the region 340–500 nm.

Table 1. Non exhaustive survey of reports dealing with ternary organic solar cells based on polymeric sensitizers. Performance of the binary and ternary solar cells is reported under AM1.5G, 100 mW/cm².

Year	Binary blend (donor:acceptor)	Binary cell (Reference)				Sensitizer	Ratio (donor: sensitizer:acceptor)	Ternary cell				Ref.
		J_{sc} [mA/cm ²]	V_{oc} [V]	FF [%]	PCE [%]			J_{sc} [mA/cm ²]	V_{oc} [V]	FF [%]	PCE [%]	
2010	P3HT:PCBM	7.1	0.57	63	2.5	PCPDTBT	0.8:0.2:1	8.02	0.62	55.4	2.8	[11]
2012	P3HT:PCBM	6.36	0.59	58	2.17	PCPDTBT + 3 vol.% DIO	1:0.2:1	12.67	0.55	48	3.33	[22]
2011	P:PCBM	3.6	0.95	47	1.6	PB	1:1:1	7.5	0.86	54	3.48	[24]
	PB:PCBM	3.8	0.86	48	1.57							
2012	P3HT:PCBM	8.6	0.57	63.6	3.1	Si-PCPDTBT	0.6:0.4:1	11	0.59	62.1	4.0	[25]
2012	P3HTT-DPP-10%: PCBM	14.38	0.57	62	5.07	P3HT ₇₅ -co-EHT ₂₅	0.9:0.1:1.1	15.05	0.60	61	5.51	[30]
	P3HT ₇₅ -co-EHT ₂₅ : PCBM	7.96	0.67	0.59	3.16							
2012	DTPyT:PCBM	12.8	0.85	58.1	6.3	DTffBT	0.5:0.5:1	13.7	0.87	58.9	7.02	[16]
	DTffBT:PCBM	12.2	0.91	56.5	6.26							
2012	TAZ:PCBM	8.68	0.75	62.4	4.06	DTBT	0.3:0.7:1	11.9	0.81	60.68	5.88	[16]
	DTBT:PCBM	10.2	0.87	49.6	4.39							
2009	P3HT:PCBM	5.16 ^{a)}	0.57	53.8	3.16	F8BT	1:1.4:0.6	3.22 ^{a)}	0.67	45.2	1.94	[31]
2011	DO-PThE1- PPV2:PCBM	4.5	0.84	41	1.6	MEH-PThE1-PPV2	0.5:0.5:3	5.7	0.86	40	2.0	[32]
	MEH-PThE1- PPV2:PCBM	4.9	0.73	36	1.3							
2011	P3HT:PCBM	7.29	0.67	46.6	2.26	FLC8	1:0.05:0.8	8.16	0.68	52.8	2.93	[33]
2012	P3HT:PCBM	13.2	0.6	55	4.1	P6	0.9975:0.0025:1	21.3	0.6	44	5.3	[34]

^{a)}Illuminated under intensity of 50 mW/cm².

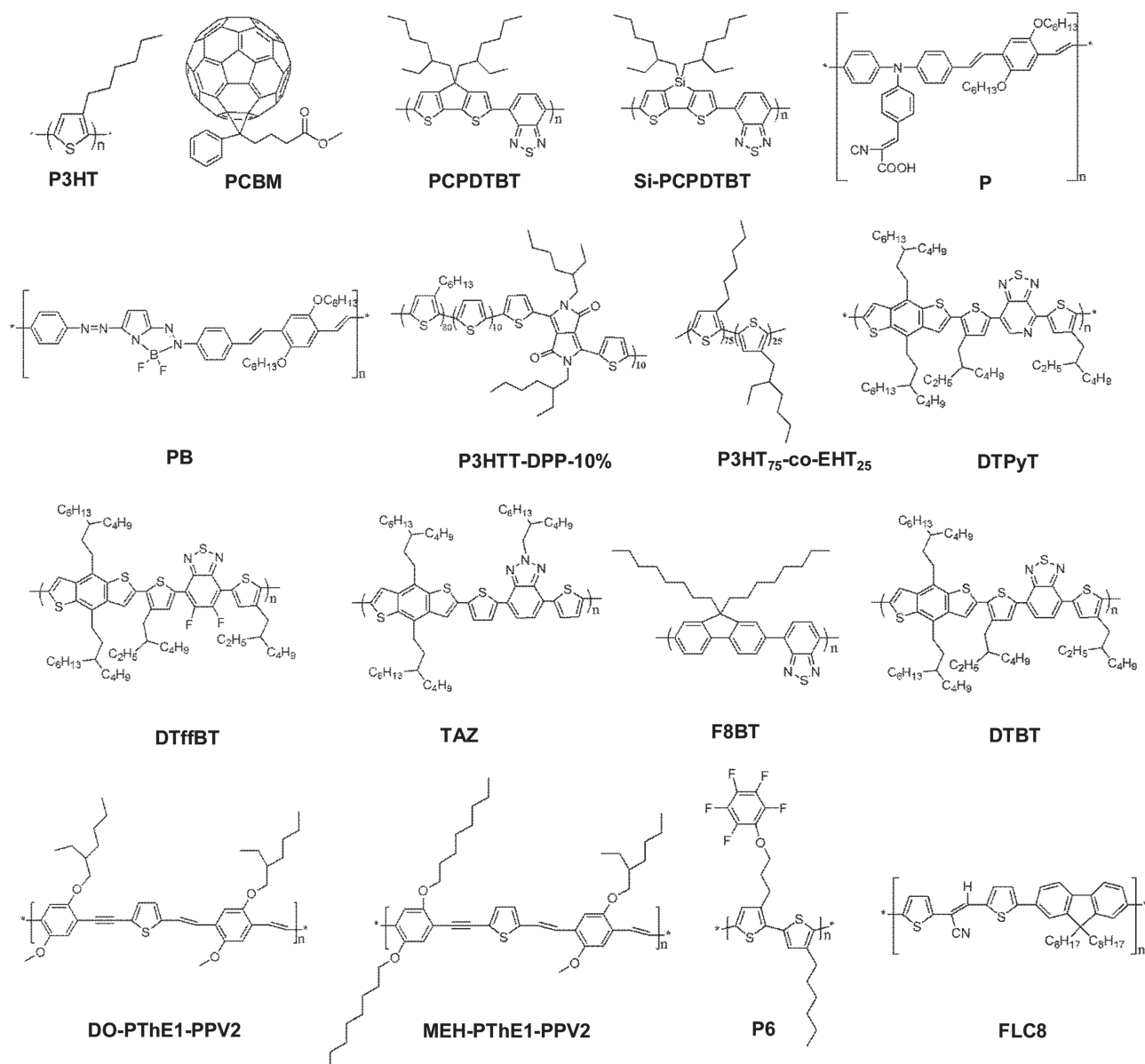


Figure 17. Chemical structures of the utilized materials in the ternary organic solar cells based on polymeric sensitizers.

where TQTFA had strong light absorption (Figure 18a). For the devices containing higher content of TQTFA, however, the values of J_{sc} and FF decreased upon increasing concentration. As a result, poor PCEs were obtained, even though the value of V_{oc} continued to increase. The observed decrease in the J_{sc} and FF values was rationalized by reduced crystallinity of the host system upon blending with a higher content of small molecules, leading to an unfavorable morphology for charge transport.

Sharma et al.^[36] introduced a small molecule containing thienothiadiazole central unit with terminal cyanovinylene 4-nitrophenyl at both sides, which were connected to the central unit via a thiophene ring (denoted as SM), into P3HT:PCBM as near IR sensitizer. The compound SM has

HOMO and LUMO levels of -5.15 and -3.45 eV, respectively, suggesting a cascade charge transfer in this ternary blend. SM exhibited an absorption band in the wavelength region of 580 – 680 nm, having the absorption edge at approximately 760 nm. An equal mixing ratio of the three components led to an efficiency improvement of 20% before thermal annealing. Further performance improvement was observed after thermal annealing, leading to a PCEs of 4.1% with $J_{sc} = 10.3$ mA/cm², $V_{oc} = 0.7$ V and FF = 57%. The EQE spectrum of the device based on P3HT:PCBM was enhanced at wavelength region of 500 – 780 nm upon blending with SM, particularly in the region above 600 nm, where SM had strong light absorption (Figure 18b).

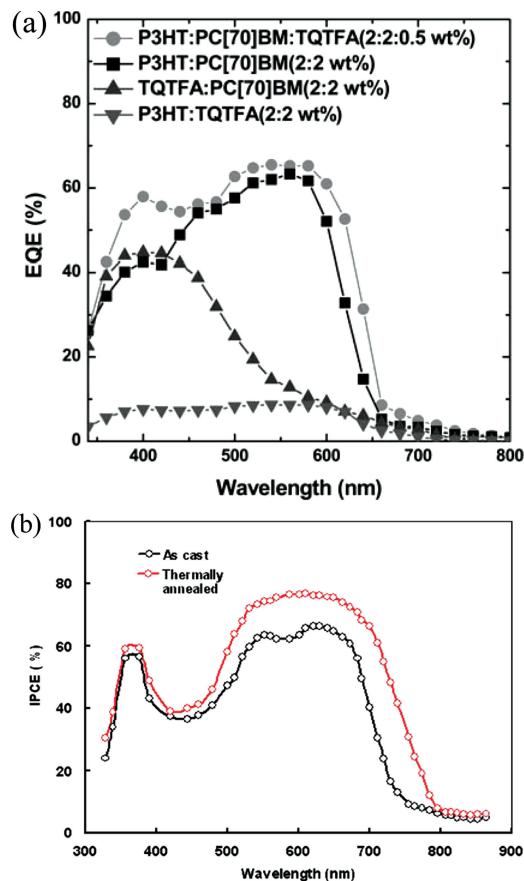


Figure 18. EQE spectra of the a) binary cell of P3HT:PC70BM, TQTFAs:PC70BM, P3HT:TQTFAs and ternary solar cell of P3HT:TQTFAs:PC70BM (2:0.5:2). Reproduced with the permission from Ref. [35] Copyright 2010, Royal Society of Chemistry; b) ternary cells of as cast and thermally annealed P3HT:SM:PCBM (1:1:1). Reproduced with the permission from Ref. [36]. Copyright 2011, Elsevier.

Sharma et al further increased the light harvesting properties of P3HT:PC70BM based solar cells by employing the near IR sensitizer DPP-CN, containing electron donor diketopyrrolopyrrole (DPP) core and cyanovinylene-4-nitrophenyl (CN).^[37] DPP-CN showed an absorption band at 550–750 nm with a peak at around 652 nm. The ternary system P3HT:DPP-CN:PC70BM possessed a cascade-type energy band structure. The best performance was observed in P3HT:PC70BM device containing 8 wt% DPP-CN, resulting in a substantially improved Jsc and FF (10.92 mA/cm² and 66%, respectively) and a slight increase in Voc (0.7 V). The corresponding PCE is 4.37%, approximately 35% higher relative to that of the binary P3HT:PC70BM. Optimizing the microstructure of the ternary blend through solvent formulation caused further improvement of the device up to 4.7% with Jsc = 12.29 mA/cm², Voc = 0.66 V and FF = 58%. The enhanced efficiency is attributed to the better ordering and therefore fewer distortions in the P3HT chains by using a mixed solvent CN/THF rather than THF.

Another DPP-based near IR sensitizer was integrated into the P3HT:PCBM by Lee et al.^[38] The energy levels of 3,6-di(4-(dimethylamino)phenyl)-2,5-di(2-decytetradecyl)-

pyrrolo[3,4-c]pyrrole-1,4-dione (DMPA-DTDPP) did meet the energetic requirements for cascade energy transfer with P3HT and PCBM. DMPA-DTDPP had a wide-ranging absorption band between 500–800 nm with two main peaks at 630 and 680 nm. The best performance observed used 5 wt% DMPA-DTDPP, which showed a substantially improved Jsc of 9.84 mA cm⁻², whereas the Voc of 0.60 V and the FF of 58% remained similar to those of that obtained for the device lacking DMPA-DTDPP. The corresponding PCE was 3.37%, approximately 12% higher relative to that of the binary P3HT:PCBM. Nevertheless, the EQE spectra of the ternary device didn't show any sensitization beyond 650 nm in the presence of DMPA-DTDPP. Addition of DMPA-DTDPP increased the EQE corresponding to the P3HT absorption (~60% at 450–550 nm). This suggests that the DMPA-DTDPP molecules are not directly involved in the photoabsorption, but contribute to photocurrent by creating a more favorable distribution of P3HT:PCBM charge generation interfaces.

Cha et al.^[39] used two anthracene-based star-shaped conjugated small molecules, 5',5''-(9,10-bis((4-hexylphenyl)ethynyl)anthracene-2,6-diyl)bis(5-hexyl-2,2'-bithiophene) (HBantHBT) and 5',5''-(9,10-bis(phenylethyne)anthracene-2,6-diyl)bis(5-hexyl-2,2'-bithiophene) (BantHBT) as UV-Vis sensitizers in two different host systems. These molecules showed a maximum absorption at ~400 nm and displayed good crystalline self-organization properties with an ordinary field-effect mobility of 5.3×10^{-3} cm²/Vs.^[40] Adding 20 wt% BantHBT into the P3HT:PCBM increased the device performance from 3% to 3.7%, while HBantHBT deteriorated the device performance compared to the reference, mainly due to Jsc reduction. On the basis of transmission electron microscopy (TEM) and X-ray diffraction scattering (GIXD) results, the small molecule HBantHBT formed separated big crystalline domains apart from those of P3HT so that this planar-like microstructure influenced the device performance negatively.

As second host matrix, the binary composite poly((5,5-E-alpha-((2-thienyl)methylene)-2-thiopheneacetonitrile)-alt-2,6-[((1,5-didecyloxy)naphthalene)]) (PBTADN):PC70BM was sensitized with HBantHBT and BantHBT. Increasing the concentration of HBantHBT kept the FF rather constant or just slightly dropped it while Jsc peaked at sensitizer concentration of 20 wt%. Integration of BantHBT increased the FF slightly up to 30 wt% and showed a small drop afterward. Jsc increased up to 20 wt% and then remained constant until 40 wt% BantHBT. At sensitizers loading of 10 wt%, Voc increased slightly and then remained constant in both ternary devices. Overall, highest PCEs were achieved at 1:0.2:4 wt% ratio of PBTADN:sensitizer:PC70BM. The device containing small molecules of HBantHBT and BantHBT exhibited high PCEs of 4.1 (Jsc = 8.7 mA/cm², Voc = 0.89 V and FF = 52.1%) and 5.6% (Jsc = 11 mA/cm², Voc = 0.91 V and FF = 56.4%), respectively, which is a considerable increase compared to the PBTADN:PC70BM reference device with the PCEs of 3%. Though the EQE spectra of the ternary solar cells presented an overall increase in comparison to that measured for reference cell, the main increase was observed in the range of 450–600 nm where the host polymer PBTADN absorbed. Large differences in the mobility ratios (μ_e/μ_h) were observed for the three systems.

Table 2. Non exhaustive survey of reports dealing with ternary organic solar cells based on small molecule sensitizers. Performance of the binary and ternary solar cells is reported under AM1.5G, 100 mW/cm².

Year	Binary Blend (donor:acceptor)	Binary cell (Reference)			Sensitizer	Ratio(donor: sensitizer:acceptor)	Ternary cell			Ref.		
		Jsc [mA/cm ²]	Voc [V]	FF [%]			Jsc [mA/cm ²]	Voc [V]	FF [%]			
2010	P3HT:PC70BM	9.74	0.6	66.6	3.9	TQTFA	2:0.5: 2	10.62	10.62	60.7	4.5	[35]
2011	P3HT:PCBM	8.0	0.68	54	2.93 ^{a)}	SM	1:1:1	9.2	0.73	55	3.69 ^{a)}	[36]
							10.3	0.70	57	57	4.1 ^{b)}	
2012	P3HT:PC70BM	9.4	0.66	52	3.23 ^{c)}	DPP-CN	1:0.08:1	10.92	0.70	58	4.37 ^{c)}	[37]
							12.29	0.66	58	58	4.7 ^{d)}	
2012	P3HT:PCBM	8.27	0.60	61	3.02	DMPA-DTDPP	1:0.05:0.8	9.84	0.60	58	3.37	[38]
2012	P3HT:PCBM	8.6	0.62	55.8	3	BantHBT	1:0.2:1	9.8	0.62	60.4	3.7	[39]
2012	PBTADN:PC70BM	6.9	0.83	53.1	3	HBantHBT	1:0.2:4	8.7	0.89	52.1	4.1	[39]
							BantHBT	1:0.2:4	11	0.91	56.4	5.6
2012	P3HT:PCBM	9.5	0.56	53	2.8	DCF1	1: 0.5: 0.5	13.5	0.61	55	4.5	[41]

^{a)}As cast; ^{b)}Thermal annealed; ^{c)}THF cast; ^{d)}THF/CN cast.

On the basis of the space charge limited current (SCLC) results, the μ_e/μ_h ratio of 147.9, 93.1, 7.94 were evaluated for the PBTADN:PC70BM, PBTADN:HBantHBT:PC70BM, and PBTADN:BantHBT:PC70BM blends, respectively. It suggests that small molecule incorporation strongly improved the percolation pathways for the hole carriers and therefore better balanced charge carrier mobilities.

Similar mechanisms were reported by Andrew et al.^[41] Implementation of different n-type 6,6-dicyanofulvenes (DCFs) into the P3HT:PCBM significantly increased J_{sc}, although DCFs themselves did not yield functional binary devices with P3HT. Substituting half of PCBM by 1,4-dimethyl-2,3-diphenyl-DCF (DCF1), which had a LUMO level of -3.8 eV and an absorption peak at ~370 nm, ternary solar cells yielded PCEs of 4.5% and a J_{sc} = 13.5 mA/cm², Voc = 0.61 V and FF = 55%.

Table 2 summarizes the performance parameters of ternary organic solar cells based on small molecule sensitizers and their corresponding reference device. A short overview of the chemical structure of the most prominent materials utilized in those devices is given in **Figure 19**.

3.3. Dye Sensitizers

Dyes are aromatic organic compounds with large absorption coefficients and exist in a vast array of colors, used nowadays in many research and industry areas. The early reported ternary solar cells containing dye sensitizers were based on thermally evaporated materials in a planar-film structure.^[42] In 2010, Mikroyannidis et al.^[43] had demonstrated ternary solar cells comprised of two solution-processed dye pigments of 2,5-Bis(2-anthracyenylidazo)-1H-pyrrole (D1) and 2,20-[1,4-phenylenebis(azo)]bis-1H-pyrrole (D2), blended into PCBM. The best performing device exhibited PCEs of about 3.61% for a thermally annealed D1:D2:PCBM (1:1:1 wt.%) photoactive layer, yielding 33% improvement compared to the

D1:PCBM reference. This ternary composite had a cascade energy level type alignment.

Multi-colored dye sensitization of P3HT:PCBM solar cells was explored by Honda et al.^[44] By selecting appropriate complementary-absorbing dyes like silicon phthalocyanine bis(triethylsilyl oxide) (SiPc) and silicon naphthalocyaninebis(triethylsilyl oxide) (SiNc), quaternary solar cells boosted the photocurrent and hence the device efficiency over the binary references. The highest PCEs of 4.3 with a J_{sc} = 10.9 mA/cm², Voc = 0.57 V and FF = 69% was obtained for a P3HT:SiPc:SiNc:PCBM quaternary solar cell (weight ratio of 1:0.048:0.015:1), while the reference cell and ternary cells containing 4.8 wt.% SiPc and 1.5 wt.% SiNc exhibited the PCEs of 3.5, 4.1 and 3.7%, respectively. The quaternary solar cells exhibited an improved EQE peak at 400–600 nm and two sharp EQE peaks at 670 and 780 nm (**Figure 20a**), corresponding to the absorption of SiPc and SiNc. Indeed, the rise in J_{sc} arose from: first, a direct contribution of the dye molecules to photogeneration (670 and 780 nm peaks) and secondly, an indirect contribution of the dye molecules via a cascade charge transfer process from those dye molecules being located at the interface between P3HT and PCBM^[45] (400–600 nm region).

Afterwards, ternary P3HT:SiPc:PCBM were investigated in great detail to gain insight into the microstructure modifications due to dye loading.^[46] Absorption and surface energy measurements proposed that SiPc molecules localized in disordered P3HT phases at the interface between P3HT and PCBM rather than in the crystal domains of PCBM and P3HT. The local concentration of SiPc ([SiPc]_{Local}) in the ternary blends was assessed from the peak wavelength of the dye absorption (λ_{max}). The local concentration of SiPc in ternary composites prepared at different conditions versus SiPc content is presented in **Figure 20b**. By mixing 3.4 wt.% SiPc dye into the regioregular P3HT:PCBM blend, the [SiPc]_{Local} was estimated to be as high as 20 wt.% before and 25 wt.% after thermal annealing. Increasing the SiPc concentration above 10 wt.%, where the [SiPc]_{Local} became saturated, a significant

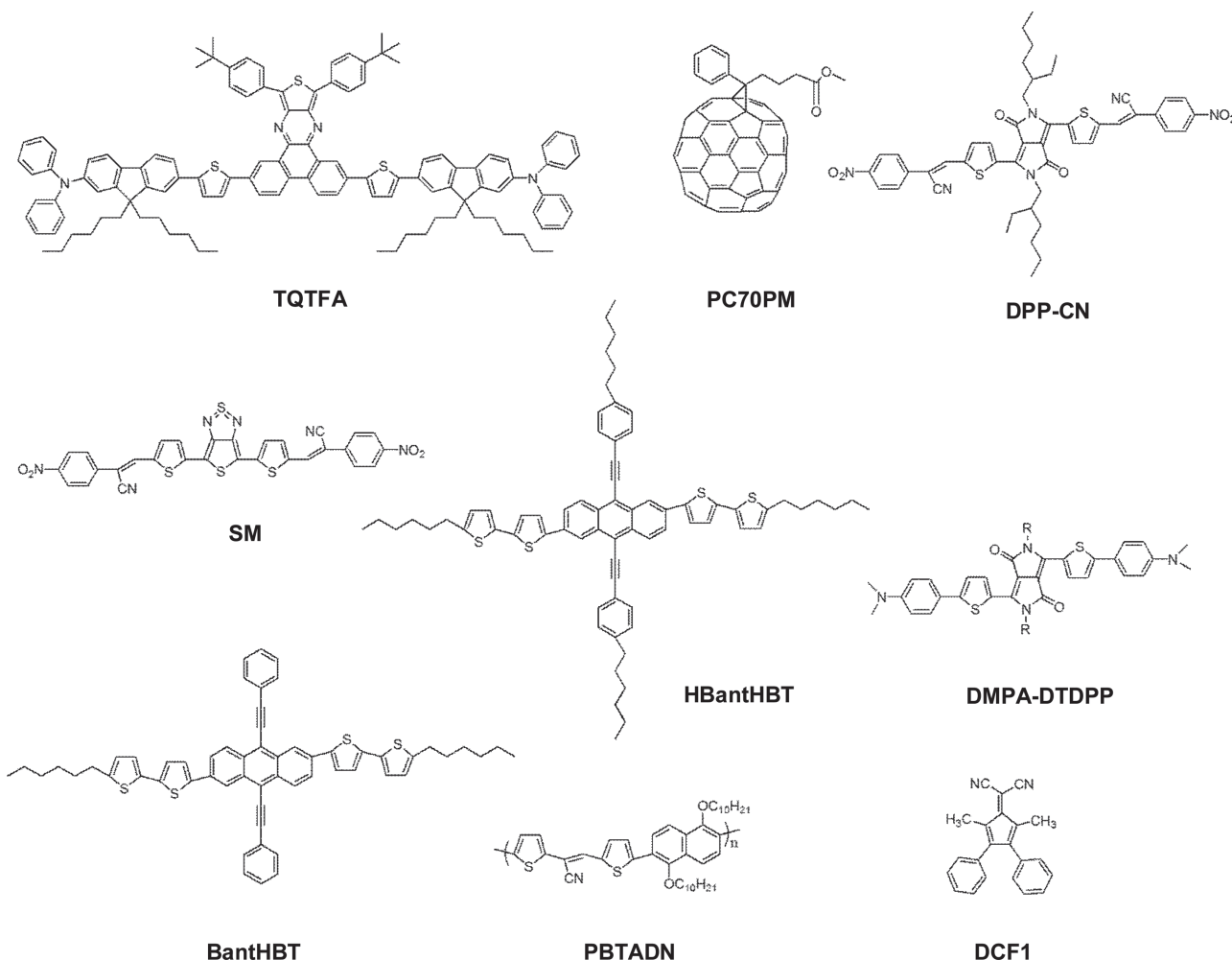


Figure 19. Chemical structures of the utilized materials in the ternary organic solar cells based on small molecule sensitizers.

performance drop was observed mainly based on J_{SC} and FF reduction. On the other hand, solvent annealed devices kept the high performance for dye loadings as high as 17 wt.%.

This difference was attributed to the separate film microstructures formed differently for each annealing method. Further increasing the dye concentration enabled immigration of

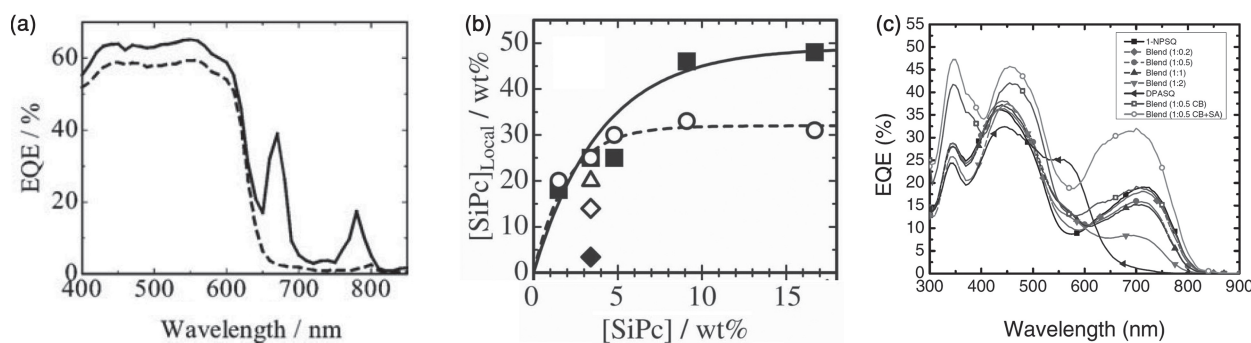


Figure 20. a) EQE spectra of the a) binary cell of P3HT:PCBM (broken lines) and quaternary cell of P3HT:SiPc:SiNc:PCBM (solid lines). Reproduced with the permission from Ref. [44], Copyright 2010. Royal Society of Chemistry; b) Local concentrations of SiPc in RRa-P3HT (closed diamond), RR-P3HT:PCBM (open diamond), and RR-P3HT:PCBM before (open triangle) and after thermal annealing (open circles) and solvent annealing (closed squares) versus the SiPc content. The solid and broken lines are guided to the eye for solvent and thermal annealing, respectively.^[46] The abbreviations of RRa and RR are correspond to regiorandom and regioregular, respectively. Reproduced with the permission from Ref. [46]; c) binary cells of DPASQ/C60 and 1-NPSQ/C60 and ternary cells of DPASQ:1-NPSQ/C60 at different donor weight ratios and different process conditions; SA: solvent annealed, CB: including compound buffer interface.^[48] Reproduced with the permission from Ref. [48].

SiPc molecules from the interface areas into the crystalline PCBM phases. Solvent annealing did not trigger such a diffusion process, and, consequently the dye molecules remained at the interface. Therefore, the solvent-annealed devices could load much more dye molecules and PCBM at the interface without negatively impacting the blend morphology. In fact, two driving forces for the aggregation of dyes at the interface of polymer/fullerene has been identified in this study: surface energy which is the primary driving force for the localization, and crystallization of the host matrix which acts as assistance to the main driving force.

Incorporation of insoluble tetramethylsubstituted copper(II) phthalocyanine (CuMePc) nanocrystals into the P3HT:PCBM matrix was demonstrated by Xu et al.^[47] The spin-coated film of the CuMePc nanocrystals exhibited two broad absorption peaks at 617 and 708 nm. Mobility measurements for P3HT:CuMePc blends showed that CuMePc nanocrystals acted as traps or impurities at low loading concentrations which deteriorated transport. Loading 25 wt.% of CuMePc, mobility of the composite film was again in par with mobility of P3HT. The composite including identical volumes of P3HT and CuMePc exhibited the high mobility of $2.5 \times 10^{-2} \text{ cm}^2/\text{Vs}$, exceeding the mobility of P3HT ($7.3 \times 10^{-3} \text{ cm}^2/\text{Vs}$). The ternary cell fabricated with a P3HT:CuMePc:PCBM (1:1:2) composite illustrated best photovoltaic performance with $J_{\text{sc}} = 16.3 \text{ mA/cm}^2$, $V_{\text{oc}} = 0.58 \text{ V}$, $\text{FF} = 56\%$ and a PCE = 5.3%, resulting in ~40% enhancement compared to the P3HT:PCBM reference. This enhancement is attributed to the higher mobility and the wider absorption of the ternary composite.

In another study, Xiao et al.^[48] demonstrated efficient ternary solar cells based on functionalized squaraine donor sensitizers. Ternary solar cells were engineered from small molecular blends consisting of (2-[4-(N,N-diphenylamino)-2,6-dihydroxyphenyl]-4-diphenylamino) (DPASQ) and the red shifted 2,4-bis[4-(N-phenyl-1-naphthylamino)-2,6-dihydroxyphenyl] squaraine (1-NPSQ), with a 40 nm thick C₆₀ layer thermally evaporated on top as the acceptor. The ternary device 1-NPSQ:DPASQ/C₆₀ with donor blending ratios of 1:0.5 wt.% reached the PCEs of 5.2%, yielding ~23 and 18% performance improvement compared to the binary reference devices. To further optimize the

device performance, the solution-processed film was solvent-vapor annealed rather than thermal annealed, leading to a PCEs of 5.9% with $J_{\text{sc}} = 10.5 \text{ mA/cm}^2$, $V_{\text{oc}} = 0.78 \text{ V}$ and $\text{FF} = 72\%$. The absorption contribution of DPASQ and 1-NPSQ small molecules to the photocurrent were revealed in the EQE spectra at wavelength ranges between 400–600 and 600–800 nm, respectively (Figure 20c). Owing to the good transport property of each small molecule, a parallel-like charge transfer/transport mechanism is proposed for these ternary solar cells.

A summary of the reports dealing with ternary organic solar cells based on dye sensitizers is given in Table 3. Figure 21 presents the chemical structures of the dye compounds.

3.4. Nanoparticle Sensitizers

Another promising approach to enhance light harvesting is hybrid composites based on inorganic nanoparticle sensitizers. Among them, metallic nanoparticles (NPs) such as Au and Ag NPs and other metallic nanostructures are discussed as potential candidates for improving the light absorption due to the localized surface plasmon resonance (LSPR). LSPR couples strongly to the incident light and thus enhances the local absorption within the vicinity of the plasmonic structure.^[49] In addition, relatively large metallic NPs can reflect and scatter light and thereby also increase the optical path length within the BHJ film.

Incorporation of the Ag NPs into the polymer:fullerene was investigated by several groups. Naidu et al.^[50] developed a hybrid ternary cell comprised of P3HT:[6,6]-phenyl C₆₁-butyric acid butyl ester (PCBB):Ag NPs. Homogenous Ag NP distribution within the photoactive layer was designed by drying P3HT:PCBB films containing silver nitrate (AgNO₃) and poly(ethylene glycol) (PEG) at 120 °C for 10 min. The formation of Ag NPs took place through the oxidation of the hydroxyl groups present in the PEG. An absorption feature observed in the range of 375–405 nm proved the presence of Ag NPs in the hybrid film. The presence of Ag NPs in the photoactive layer led to higher absorption but also to higher charge carrier mobility of the hybrid film. As a result, PCEs of 4.08% were obtained. As depicted in Figure 22a, an EQE maximum of 70% at 520 nm

Table 3. Non exhaustive survey of reports dealing with ternary organic solar cells based on dye sensitizers. Performance of the binary and ternary solar cells is reported under AM1.5G, 100 mW/cm².

Year	Binary Blend (donor:acceptor)	Binary cell (Reference)				Sensitizer	Ratio (donor: sensitizer:acceptor)	Ternary cell				Ref.
		J_{sc} [mA/cm ²]	V_{oc} [V]	FF [%]	PCE [%]			J_{sc} [mA/cm ²]	V_{oc} [V]	FF [%]	PCE [%]	
2010	D1:PCBM	6.12	0.84	51	2.62	D2	1:1:1	7.60	0.85	56	3.61	[43]
	D2:PCBM	5.5	0.93	41	2.1							
2010	P3HT:PCBM	8.96	0.55	71	3.5	SiPc	1:0.048:1	10.3	0.57	69	4.1	[44]
						SiNc	1:0.015:1	9.94	0.55	68	3.7	
						SiPc: SiNc	1:0.048:0.015:1	10.9	0.57	69	4.3	
2011	P3HT:CBM	9.69	0.55	66	3.5 ^{a)}	SiPc	1:0.048:1	11.1	0.58	65	4.2 ^{a)}	[46]
2011	P3HT:PCBM	10.7	0.61	50	3.2	CuMePc	0.5:0.5:1	16.3	0.58	56	5.3	[47]
2012	DPASQ/C ₆₀	5.5	1	72	4 ^{b)}	1-NPSQ	0.5:1/C ₆₀	7.3	0.98	71	5.1 ^{b)}	[48]
	1-NPSQ/C ₆₀	6.8	0.92	70	4.4 ^{b)}			10.5	0.78	72	5.9 ^{a,c)}	

^{a)}Solvent annealing; ^{b)}As cast; ^{c)}Compound buffer interface.

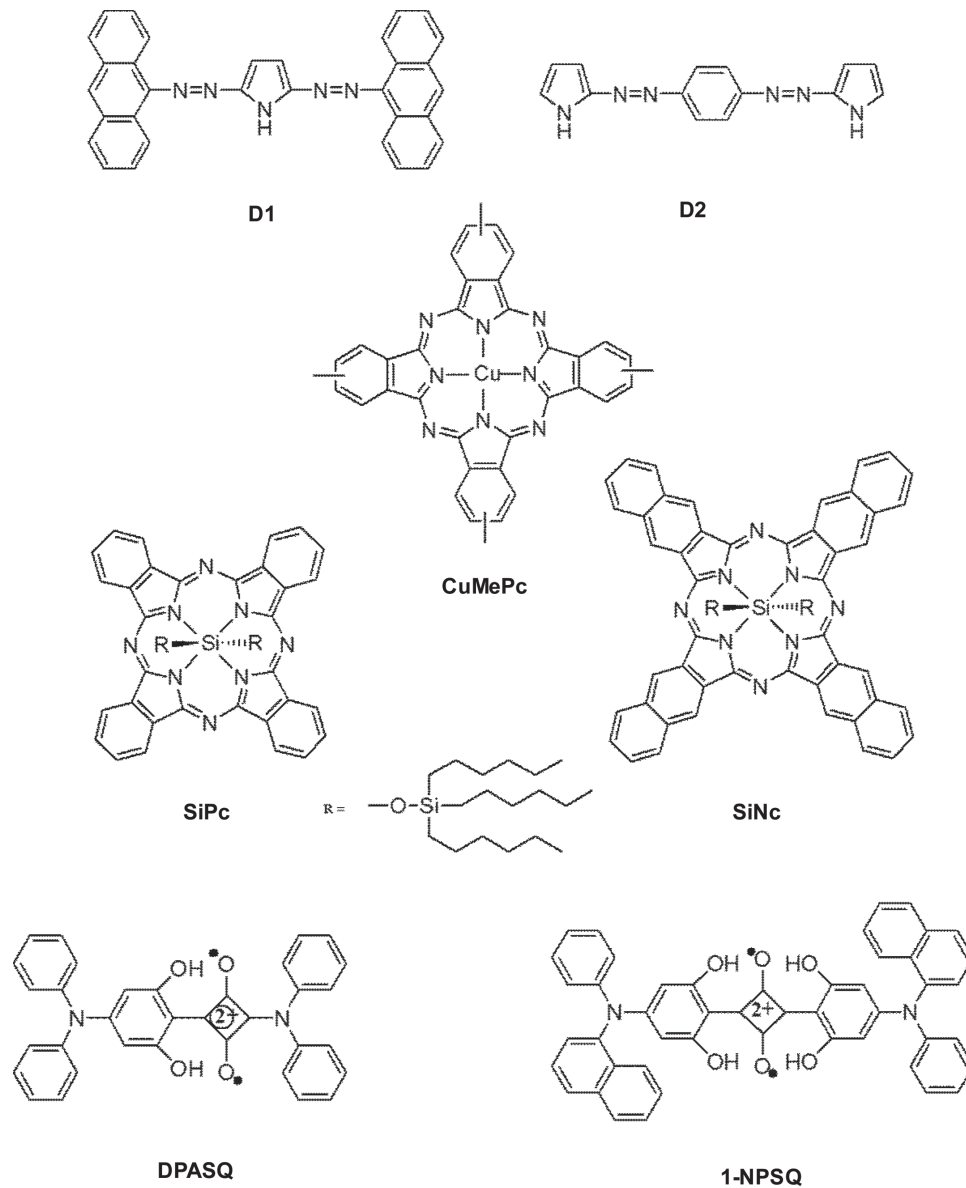


Figure 21. Chemical structures of the utilized dye compounds in the ternary organic solar cells.

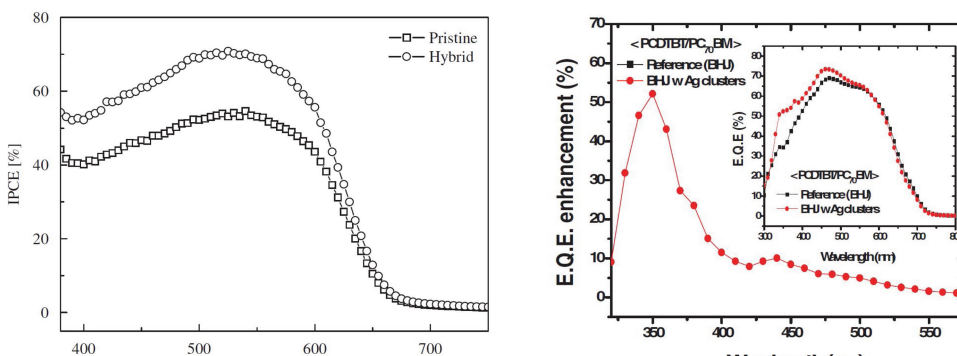
was observed for the ternary cell, while the binary P3HT:PCBB reference had a maximum of only 51% at the same wavelength. Replacing PEDOT:PSS as hole extraction layer with the highly conductive glycerol-modified PEDOT:PSS further improved the efficiency up to 4.3% with a $J_{sc} = 12.29 \text{ mA/cm}^2$, $V_{oc} = 0.64 \text{ V}$ and $FF = 54.6\%$.

Similar results were reported by Li et al.^[51], where the P3HT:PCBM was sensitized by a mixture of Ag NPs and Ag nanoprisms. Theoretical as well as experimental studies revealed that especially the Ag nanoprisms have improved overlap with absorption spectrum of P3HT Ternary devices containing 2 wt.% Ag NPs and 2 wt.% nanoprisms resulted in PCEs of 4.3%, an improvement of around 20%.

The influence of Ag NPs size on the performance of poly[N-9'-hepta-decanyl-2,7-carbazole-alt-5,5-(4',7'-di-2-thienyl-2',1'-benzothiadiazole)] (PCDTBT):PC70BM solar cells was studied by

Wang et al.^[52] They observed the formation of Ag clusters from individual Ag NPs in the BHJ composite during film casting and drying. At an optimized blend ratio of 1 wt.% with 40 nm-sized NPs based Ag clusters in PCDTBT:PC70 BM, the PCE increased from 6.3% to 7.1% with the $J_{sc} = 11.61 \text{ mA/cm}^2$, $V_{oc} = 0.88 \text{ V}$ and $FF = 69\%$. The inset of Figure 22b shows that optimized devices with Ag clusters exceeded an EQE of over 75% near 450 nm. Moreover, as shown in Figure 22b, EQE enhancement is observed in the wavelength range of 350 nm to 550 nm for the hybrid ternary device containing Ag clusters..This performance enhancement is attributed to enhanced light absorption as well as improved charge transport in the photoactive layer.

Other metallic nanostructures have shown very similar impact on the organic BHJ solar cells. For instance, implementation of mono-functional poly(ethylene glycol) (PEG)-capped Au NPs into the blend of



(a)

(b)

Figure 22. a) EQE spectra of the binary cell of P3HT:PCBB (square) and ternary cell of P3HT:Ag NPs:PCBB (circle). Reproduced with the permission from Ref. [50]. Copyright 2008, Elsevier; b) EQE enhancement spectra of the ternary devices PCDTBT:PC70BM including the 40 nm-sized NPs based Ag clusters (1 wt.%). The inset figure shows measured EQE of the PCDTBT:PC70BM binary reference cell (square) and ternary cell with Ag clusters (circle)^[52] Reproduced with the permission from the Ref. [52].

poly[2,7-(9,9-dioctylfluorene)-alt-2-((4-(diphenylamino) phenyl thiophen-2-yl)malononitrile] (PFSDCN):PCBM improved the PCE by ~32%.^[53] A PCE of 2.17% was achieved for an optimized Au NPs concentration to 0.5 wt.%. Furthermore, based on theoretical simulation, Au NPs were shown to enhance light absorption due to a dominant lateral distribution of the LSPR near field along the photoactive layer rather than a vertical distribution across the active layer.

Enhancement of the efficiency by integration of Au NPs into the various polymer:fullerene BHJ solar cells was further reported by Wang et al.^[54] At the optimized blend ratio of 5 wt.% Au NPs in P3HT:PC70BM, the PCE increased from 3.54% to 4.36%. Similar mixing ratios increased the performance, from 5.77% to 6.45% for PCDTBT:PC70BM and from

3.92% to 4.54% for Si-PCPDTBT:PC70BM solar cells. Multiple scattering from the large Au NPs (70 nm) and therefore longer optical paths within the BHJ photoactive layer were suggested as the dominant mechanism for enhanced performance.

Finally, sensitization through semiconductor nanostructures was suggested to enhance the light harvesting properties of organic solar cells. The absorption wavelength of semiconductor nanostructures can be tuned according to their size, composition and shape,^[55] and thus can be well tuned to match the solar radiation spectrum. Recently, Fu et al.^[56] demonstrated sensitization of P3HT:PCBM solar cells with CdSe quantum dots. The incorporation of 10 wt.% CdSe quantum dots increased the PCE to 3.05% compared to the 2.06% efficiency for the binary reference.

Table 4. Non exhaustive survey of reports dealing with ternary organic solar cells based on nanoparticle sensitizers. Performance of the binary and ternary solar cells is reported under AM1.5G, 100 mW/cm².

Year	Binary cell (donor:acceptor)	Binary cell (Reference)				Sensitizer NP size [nm]	Ratio (donor: sensitizer:acceptor)	Ternary cell				Ref.
		J _{sc} [mA/cm ²]	V _{oc} [V]	FF [%]	PCE [%]			J _{sc} [mA/cm ²]	V _{oc} [V]	FF [%]	PCE [%]	
2008	P3HT:PCBB	9.54	0.61	59.1	3.43 ^{a)}	Ag NPs	1:0.045:0.7	10.84	0.60	62.3	4.08 ^{a)}	[50]
								12.29	0.64	54.6	4.3 ^{b)}	
2013	P3HT: PCBM	8.99	0.64	62.33	3.60	Ag NPs (20)	1:0.02:1	9.80	0.64	63.58	3.99	[51]
						Ag nanoprisms (60)	1:0.02:1	9.93	0.64	64.08	4.07	
						Ag NPs+nanoprisms	1:0.02 + 0.02:1	10.61	0.64	63.33	4.30	
2011	PCDTBT:PC70BM	10.79	0.86	68	6.3	Ag NPs (40)	1:0.01:4	11.61	0.88	69	7.1	[52]
2011	PFSDCN:PCBM	-	0.9	-	1.64	Au NPs (10–100 nm)	-:0.05:-	-	1.01	-	2.17	[53]
2011	P3HT:PC70BM	10.65	0.57	57	3.49	Au NPs (70)	1:0.05:0.6	11.08	0.63	62	4.31	[54]
	PCDTBT:PC70BM	-	-	64	5.77		1:0.05:4	11.16	0.89	65	6.45	
	Si-PCPDTBT: PC70BM	-	-	63	3.92		1:0.05:2	13.13	0.57	61	4.54	
2012	P3HT:PCBM	7.51	0.57	48	2.06	CdSe	1:0.1:1	8.15	0.60	62	3.05	[56]

^{a)}Buffer Layer = PEDOT:PSS; ^{b)}Buffer Layer = Glycerol-PEDOT:PSS.

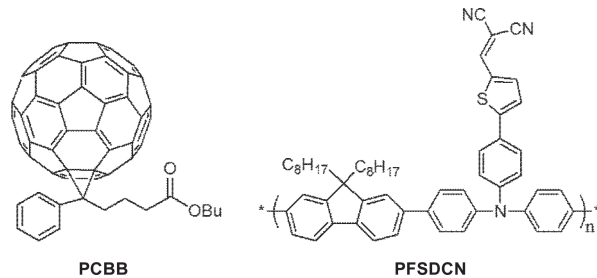


Figure 23. Chemical structures of the new utilized materials in the ternary organic solar cells based on nanoparticle sensitizers.

Further insight into the sensitization mechanisms with semiconductor nanostructures is in progress.^[57]

A summary of the NPs sensitized BHJ solar cells are provided in Table 4. The corresponding chemical structures are shown in Figure 23.

4. Summary and Outlook

The novel and smart concept of ternary organic solar cells is a promising approach to extend the limited absorption spectrum of organic semiconductors into the near IR region, thus enhancing the light harvesting properties as well as the power performance. In this regard, various types of sensitizers such as low bandgap polymers, small molecules, dyes or nanoparticles are discussed as third component for BHJ polymer:fullerene solar cells. The concentration of the sensitizer is decisively impacting the microstructure formation, while the respective energy level alignment is decisive for the sensitization mechanism. Cascade charge transfer, parallel-like charge transfer and energy transfer reactions are among the most relevant mechanisms for successful sensitization. To date, the most efficient ternary organic solar cell exhibited PCEs of over 7%, showing wide range absorption of 400–850 nm. Results reported so far revealed that the appropriate selection of the sensitizer offers multiple benefits like promoted exciton dissociation at the interface or improved charge carrier mobility. To gain deeper insight into the working principles of ternary organic solar cells, further fundamental research is required. A comprehensive understanding, optimized materials and evident design rules for ternary photovoltaics will pave the path towards the higher efficiencies in single junction OPVs.

Acknowledgements

The authors are grateful to the German Research Foundation (DFG, grant No. BR 4031/2-1) and the Solar Technologies go Hybrid (SolTech) projects for financial support.

Received: February 5, 2013
Published online: May 24, 2013

[1] a) M. A. Green, K. Emery, Y. Hishikawa, W. Warta, E. D. Dunlop, *Prog. Photovolt: Res. Appl.* **2012**, *20*, 606; b) http://www.heliatek.com/wp-content/uploads/2013/01/130116_PR_Heliatek_achieves_record_cell_efficiency_for_OPV.pdf.

- [2] a) C. Deibel, V. Dyakonov, *Rep. Prog. Phys.* **2010**, *73*, 096401; b) J. Frenkel, *Phys. Rev.* **1931**, *37*, 17; c) W. Y. Liang, *Phys. Education* **1970**, *5*, 226.
- [3] M. C. Scharber, D. Mühlbacher, M. Koppe, P. Denk, C. Waldauf, J. Heeger, C. J. Brabec, *Adv. Mater.* **2006**, *18*, 789.
- [4] B. Minnaert, M. Burgelman, *Prog. Photovolt: Res. Appl.* **2007**, *15*, 741.
- [5] a) M. C. Scharber, M. Koppe, J. Gao, F. Cordella, M. A. Loi, P. Denk, M. Morana, H. J. Egelhaaf, K. Forberich, G. Dennler, R. Gaudiana, D. Waller, Z. Zhu, X. Shi, C. J. Brabec, *Adv. Mater.* **2010**, *22*, 367; b) A. J. Moulé, A. Tsami, T. W. Bünnagel, M. Forster, N. M. Kronenberg, M. Scharber, M. Koppe, M. Morana, C. J. Brabec, K. Meerholz, U. Scherf, *Chem. Mater.* **2008**, *20*, 4045; c) H. Zhou, L. Yang, W. You, *Macromolecules* **2012**, *45*, 607.
- [6] a) T. Ameri, G. Dennler, C. Lungenschmied, C. J. Brabec, *Energy Environ. Sci.* **2009**, *2*, 347; b) T. Ameri, N. Li, C. J. Brabec, *Energy Environ. Sci.* **2013**, in press; c) J. You, L. Dou, K. Yoshimura, T. Kato, K. Ohya, T. Moriarty, K. Emery, C.-C. Chen, J. Gao, G. Li, Y. Yang, *Nat. Commun.* **2013**, *4*, 1446.
- [7] S. Shockley, H. J. Queisser, *J. Appl. Phys.* **1961**, *32*, 510.
- [8] M. T. Dang, L. Hirsch, G. Wantz, *Adv. Mater.* **2011**, *23*, 3597.
- [9] M. Koppe, H. J. Egelhaaf, G. Dennler, M. C. Scharber, C. J. Brabec, P. Schilinsky, C. N. Hoth, *Adv. Funct. Mater.* **2010**, *20*, 338.
- [10] H. Lösslein, T. Ameri, G. J. Matt, M. Koppe, H.-J. Egelhaaf, A. Troeger, V. Sgobba, D. M. Guldi, C. J. Brabec, "Transient Absorption Spectroscopy Studies on Polythiophene Fullerene Bulk Heterojunction Organic Blend Films Sensitized with a Low Band Gap Polymer", Accepted by *Macromol. Rapid Commun.*
- [11] M. Koppe, H.-J. Egelhaaf, E. Clodic, M. Morana, L. Lüer, A. Troeger, V. Sgobba, D. Guldi, T. Ameri, C. J. Brabec, *Adv. Energy Mater.* **2013**, DOI: 10.1002/aenm.201201076.
- [12] P.-C. Cheng, *Handbook Of Biological Confocal Microscopy*, Third edition (Ed: James B. Pawley), Springer, New York **2006**, Ch. 8.
- [13] V. Helms, *Principles of Computational Cell Biology*, Wiley-VCH, Weinheim, Germany **2008**, Ch. 8.
- [14] a) S. Honda, S. Yokoya, H. Ohkita, H. Benten, S. Ito, *J. Phys. Chem. C* **2011**, *115*, 11306; b) S. Ito, H. Ohkita, H. Benten, S. Honda, *AMBIO* **2012**, *41*(Supplement 2), 132.
- [15] H. C. Hesse, J. Weickert, C. Hundschell, X. Feng, K. Müllen, B. Nickel, A. J. Mozer, L. Schmidt-Mende, *Adv. Energy Mater.* **2011**, *1*, 861.
- [16] L. Yang, H. Zhou, S. C. Price, W. You, *J. Am. Chem. Soc.* **2012**, *134*, 5432.
- [17] H. Zhou, L. Yang, A. C. Stuart, S. C. Price, S. Liu, W. You, *Angew. Chem. Int. Ed.* **2011**, *50*, 2995.
- [18] H. Zhou, L. Yang, S. C. Price, K. J. Knight, W. You, *Angew. Chem., Int. Ed.* **2010**, *49*, 7992.
- [19] F. Machui, S. Abbott, D. Waller, M. Koppe, C. J. Brabec, *Macromol. Chem. Phys.* **2011**, *212*, 2159.
- [20] N. Li, F. Machui, D. Waller, M. Koppe, C. J. Brabec, *Sol. Energ. Mat. Sol. C* **2011**, *95*, 3465.
- [21] F. Machui, S. Rathgeber, N. Li, T. Ameri, C. J. Brabec, *J. Mater. Chem.* **2012**, *22*, 15570.
- [22] Z. Hu, S. Tang, A. Ahlvers, S. I. Khondaker, A. J. Gesquiere, *Appl. Phys. Lett.* **2012**, *101*, 053308.
- [23] a) J. Peet, J. Y. Kim, N. E. Coates, W. L. Ma, D. Moses, A. J. Heeger, G. C. Bazan, *Nat. Mater.* **2007**, *6*, 497; b) J. K. Lee, W. L. Ma, C. J. Brabec, J. Yuen, J. S. Moon, J. Y. Kim, K. Lee, G. C. Bazan, A. J. Heeger, *J. Am. Chem. Soc.* **2008**, *130*, 3619.
- [24] J. A. Mikroyannidis, D. V. Tsagkournos, P. Balraju, G. D. Sharma, *J. Power Sources* **2011**, *196*, 2364.
- [25] T. Ameri, J. Min, N. Li, F. Machui, D. Baran, M. Forster, K. J. Schottler, D. Dolfen, U. Scherf, C. J. Brabec, *Adv. Energy Mater.* **2012**, *2*, 1198.
- [26] P. P. Khlyabich, B. Burkhardt, B. C. Thompson, *J. Am. Chem. Soc.* **2011**, *133*, 14534.

- [27] S. M. Sze, *Physics of Semiconductor Devices*, 2nd Ed., Wiley-Interscience, John Wiley & Sons, USA **1981**, Ch. 14.
- [28] C. W. Schlenker, V. S. Barlier, S. W. Chin, M. T. Whited, R. E. McAnally, S. R. Forrest, M. E. Thompson, *Chem. Mater.* **2011**, *23*, 4132.
- [29] R. A. Street, D. Davies, P. P. Khlyabich, B. Burkhardt, B. C. Thompson, *J. Am. Chem. Soc.* **2013**, *135*, 986.
- [30] P. P. Khlyabich, B. Burkhardt, B. C. Thompson, *J. Am. Chem. Soc.* **2012**, *134*, 9074.
- [31] H. Kim, M. Shin, Y. Kim, *J. Phys. Chem. C* **2009**, *113*, 1620.
- [32] G. Adam, A. Pivrikas, A. M. Ramil, S. Tadesse, T. Yohannes, N. S. Sariciftci, D. A. M. Egbe, *J. Mater. Chem.* **2011**, *21*, 2594.
- [33] M. C. Chen, D. J. Liaw, Y. C. Huang, H. Y. Wu, Y. Tai, *Sol. Energ. Mat. Sol. C* **2011**, *95*, 2621.
- [34] J. M. Lobež, T. L. Andrew, V. Bulovič, T. M. Swager, *ACS Nano* **2012**, *6*, 3044.
- [35] J.-H. Huang, M. Velusamy, K.-C. Ho, J.-T. Lin, C.-W. Chu, *J. Mater. Chem.* **2010**, *20*, 2820.
- [36] S. S. Sharma, G. D. Sharma, J. A. Mikroyannidis, *Sol. Energy Mat. Sol. C* **2011**, *95*, 1219.
- [37] G. D. Sharma, S. P. Singh, M. S. Roy, J. A. Mikroyannidis, *Org. Electron.* **2012**, *13*, 1756.
- [38] J. Lee, M. H. Yun, J. Kim, J. Y. Kim, C. Yang, *Macromol. Rapid Commun.* **2012**, *33*, 140.
- [39] H. Cha, D. S. Chung, S. Y. Bae, M.-J. Lee, T. K. An, J. Hwang, K. H. Kim, Y.-H. Kim, D. H. Choi, C. E. Park, *Adv. Funct. Mater.* **2012**, DOI: 10.1002/adfm.201201913.
- [40] S. Y. Bae, S. Y. Jo, K. H. Kim, T. W. Lee, D. H. Choi, *Mol. Cryst. Liq. Cryst.* **2011**, *538*, 175.
- [41] T. L. Andrew, V. Bulović, *ACS Nano* **2012**, *6*, 4671.
- [42] a) S. Uchida, J. Xue, B. P. Rand, S. R. Forrest, *Appl. Phys. Lett.* **2004**, *84*, 4218; b) J. Dai, X. Jiang, H. Wang, D. Yan, *Appl. Phys. Lett.* **2007**, *91*, 253503; c) S. Sista, Y. Yao, Y. Yang, M. L. Tang, Z. Bao, *Appl. Phys. Lett.* **2007**, *91*, 223508.
- [43] J. A. Mikroyannidis, D. V. Tsagkournos, S. S. Sharma, A. Kumar, Y. K. Vijay, G. D. Sharma, *Sol. Energ. Mat. Sol. C* **2010**, *94*, 2318.
- [44] S. Honda, H. Ohkita, H. Benten, S. Ito, *Chem. Commun.* **2010**, *46*, 6596.
- [45] S. Honda, T. Nogami, H. Ohkita, H. Benten, S. Ito, *ACS Appl. Mater. Interfaces* **2009**, *1*, 804.
- [46] S. Honda, H. Ohkita, H. Benten, S. Ito, *Adv. Energy Mater.* **2011**, *1*, 588.
- [47] Z. X. Xu, V. A. L. Roy, K. H. Low, C. M. Che, *Chem. Commun.* **2011**, *47*, 9654.
- [48] X. Xiao, G. D. Wei, S. Y. Wang, J. D. Zimmerman, C. K. Renshaw, M. E. Thompson, S. R. Forrest, *Adv. Mater.* **2012**, *24*, 1956.
- [49] a) H. A. Atwater, A. Polman, *Nat. Mater.* **2010**, *9*, 205; b) J. R. Cole, N. J. Halas, *Appl. Phys. Lett.* **2006**, *89*, 153120; c) S.-S. Kim, S.-I. Na, J. Jo, D.-Y. Kim, Y.-C. Nah, *Appl. Phys. Lett.* **2008**, *93*, 073307; d) C. Min, J. Li, G. Veronis, J.-Y. Lee, S. Fan, P. Peumans, *Appl. Phys. Lett.* **2010**, *96*, 133302; e) W. E. I. Sha, W. C. H. Choy, W. C. Chew, *Opt. Lett.* **2011**, *36*, 478; f) W. E. I. Sha, W. C. H. Choy, W. C. Chew, *Opt. Express* **2010**, *18*, 5993.
- [50] B. V. K. Naidu, J. S. Park, S. C. Kim, S. M. Park, E. J. Lee, K. J. Yoon, S. J. Lee, J. W. Lee, Y. S. Gal, S. H. Jin, *Sol. Energy Mat. Sol. C* **2008**, *92*, 397.
- [51] X. Li, W. C. H. Choy, H. Lu, W. E. I. Sha, A. H. P. Ho, *Adv. Funct. Mater.* **2013**, DOI: 10.1002/adfm.201202476.
- [52] D. H. Wang, K. H. Park, J. H. Seo, J. Seifter, J. H. Jeon, J. K. Kim, J. H. Park, O. O. Park, A. J. Heeger, *Adv. Energy Mater.* **2011**, *1*, 766.
- [53] C. C. D. Wang, W. C. H. Choy, C. Duan, D. D. S. Fung, W. E. I. Sha, F.-X. Xie, F. Huang, Y. Cao, *J. Mater. Chem.* **2012**, *22*, 1206.
- [54] D. H. Wang, D. Y. Kim, K. W. Choi, J. H. Seo, S. H. Im, J. H. Park, O. O. Park, A. J. Heeger, *Angew. Chem. Int. Ed.* **2011**, *50*, 5519.
- [55] C. B. Murray, C. R. Kagan, M. G. Bawendi, *Annu. Rev. Mater. Sci.* **2000**, *30*, 545.
- [56] H. H. Fu, M. J. Choi, W. L. Luan, Y. S. Kim, S. T. Tu, *Solid State Electron.* **2012**, *69*, 50.
- [57] a) D. Jarzab, K. Szendrei, M. Yarema, S. Pichler, W. Heiss, M. A. Loi, *Adv. Funct. Mater.* **2011**, *21*, 1988; b) G. Itskos, A. Othonos, T. Rauch, S. F. Tedde, O. Hayden, M. V. Kovalenko, W. Heiss, S. A. Choulis, *Adv. Energy Mater.* **2011**, *1*, 802.